Interplay between the poly(A) tail, poly(A)-binding protein and coronavirus nucleocapsid protein regulates gene expression of the coronavirus and host cell

Tsung-Lin Tsai[1], Ching-Houng Lin[1], Chao-Nan Lin[2], Chen-Yu Lo[1], Hung-Yi Wu[1*]

1 Graduate Institute of Veterinary Pathobiology, College of Veterinary Medicine, National Chung Hsing University, Taichung 40227, Taiwan

2 Department of Veterinary Medicine, National Pingtung University of Science and Technology, Neipu, Pingtung 91201, Taiwan

*Corresponding Author

Keywords: coronaviruses; RNA synthesis; replication; translation; nucleocapsid protein; poly(A)-binding protein; poly(A) tail; gene expression

Corresponding Footnote: Graduate Institute of Veterinary Pathobiology, College of Veterinary Medicine, National Chung-Hsing University, Taichung, Taiwan

Telephone: 886-4-22840369; Fax: 886-4-22862073

Email: hwu2@dragon.nchu.edu.tw

Manuscript information: 136 characters in title; 225 words in abstract (250 limit) and 111 words in importance (150 limit); 40 typed manuscript pages; 9 Figures.

ABSTRACT

In the present study, we investigated the roles of interactions among poly(A) tail, coronavirus nucleocapsid (N) protein and poly(A)-binding protein (PABP) in the regulation of coronavirus gene expression. Through dissociation constant (K_d) comparison, we found that the coronavirus N protein can bind to the poly(A) tail with high affinity, establishing N protein as a PABP. A subsequent analysis with UV cross-linking and immunoprecipitation revealed that the N protein is able to bind to the poly(A) tail in infected cells. Further examination demonstrated that poly(A) tail binding by the N protein negatively regulates translation of coronaviral RNA and host mRNA both *in vitro* and in cells. Although the N protein can interact with PABP and eIF4G, the poor interaction efficiency between the poly(A)-bound N protein and eIF4E may explain the observed decreased translation efficiency. In addition to interaction with translation factor eIF4G, the N protein is able to interact with coronavirus nonstructural protein 9 (nsp9), a replicase protein required for replication. Together, the study demonstrates interactions among the poly(A) tail, N protein and PABP both *in vitro* and in infected cells. Of the interactions, binding of poly(A) tail to N protein decreases the interaction efficiency between the poly(A) tail and eIF4E, leading to translation inhibition. The poly(A)-dependent translation inhibition by N protein has not been previously demonstrated and thus extends our understanding of coronavirus gene expression.

IMPORTANCE Gene expression in coronavirus is a complicated and dynamic process. In this study, we demonstrate coronavirus N protein is able to bind to the poly(A) tail with high affinity, establishing N protein as a PABP. We also show how the interplay between coronavirus 3'-poly(A) tail, PABP and N protein regulates gene expression of the coronavirus and host cell. Of the interactions, poly(A) tail binding

by the N protein negatively regulates translation and, to our knowledge, this inhibition of translation by binding of the N protein to poly(A) tail has not been previously studied. Accordingly, the study provides fundamental molecular details regarding coronavirus infection and expands our knowledge of coronavirus gene expression.

INTRODUCTION

Members of the family *Coronaviridae*, order *Nidovirales*, are single-stranded, positive-sense RNA viruses with the largest known viral RNA genome, 26-32 kilobases (kb) (1-3). The coronavirus genome consists of a 5' cap, a 5' untranslated region (UTR), open reading frames (ORFs), a 3' UTR and a 3' poly(A) tail. The 5' two-thirds of the genome consists of two ORFs (ORF 1a and ORF 1b) that encodes 16 nonstructural proteins (nsps) with replicase activity. The other one-third of the genome largely consists of genes encoding structural proteins (3). During coronavirus infection, in addition to the replication of genomic RNA, coronaviruses synthesize a 3'-coterminal nested set of subgenomic mRNAs (sgmRNAs) from which the 5'-most ORF is translated (3).

The nucleocapsid (N) protein of coronaviruses, with a molecular weight of 50 to 55 kDa, is abundantly produced during infection. It has been shown that N protein binds to different sites of the coronaviral RNA genome with various binding affinities (4-7). Furthermore, the binding of N protein to coronaviral RNA is more efficient than to non-coronaviral RNA (6); however, it has yet to be examined whether coronavirus N protein is able to bind to the poly(A) tail. In addition to its structural role in the formation of ribonucleoprotein, N protein has been shown to interact with coronaviral replicase proteins including nsps 2-3, nsp5, nsp8 and nsps 12-13 (8-14) and is required for efficient replication (15-19). Coronavirus nsp9 is a replicase protein and has been shown to be associated with polymerase nsp12 (20), essential for replication (21) and involved in the initiation of (-)-strand RNA synthesis (22); however, whether nsp9 is able to interact with N protein remains unknown.

Poly(A)-binding protein (PABP), a 70-kDa cellular protein, is a ubiquitous cytosolic protein (23, 24). The binding of PABP to mRNA poly(A) tails is followed by interactions with eIF4G and other translation factors including eIF4E to constitute

a translation initiation complex, which mediates cellular mRNA circularization and enhances cap-dependent translation by facilitating ribosome recycling (24-26). The positive-strand coronavirus genome contains an m7GpppN-cap structure at the 5'-end and a poly(A) tail at the 3'-end, which are presumed to initiate translation in a way similar to that for cellular mRNA (3).

During coronavirus infection, the positive-strand genome functions as a template for both the synthesis of viral proteins and replication of the genome. Accordingly, a conflict may occur between the translation and replication machineries, as the ribosomes are moving along the viral RNA in the 5' to 3' direction and the viral RNA polymerase is moving in the opposite direction (3' to 5'). Therefore, a balance between these two processes must exist to enable efficient viral gene expression. In poliovirus, it has been demonstrated that the 5'-terminal cloverleaf on the viral genome functions as a regulator to control the use of the genome for translation or replication (27, 28). Binding of poly(C)-binding protein (PCBP) to this RNA structure facilitates viral translation (IRES-dependent translation), whereas interaction of the viral protein 3CD with this RNA structure represses translation and enhances replication. However, for coronaviruses, which employ a different translation mechanism (cap-dependent translation) from that of poliovirus, the strategy for coordinating the use of the positive-sense genome for translation or replication has yet to be determined.

In this study, we show that the bovine coronavirus (BCoV) N protein can bind to a poly(A) tail with high affinity. We also demonstrate that poly(A) tail binding by the N protein negatively regulates translation of coronaviral RNA and host mRNA. Finally, we demonstrate interactions among the poly(A) tail, PABP and N followed by interactions with eIF4G, eIF4E and nsp9. Based on these data, we propose a model explaining how these interactions regulate gene expression during coronavirus

131 infection.

132

133 **RESULTS**

134 **Coronavirus N protein binds to poly(A) tail with high affinity.** It has been shown
135 that N protein binds to different sites of the coronaviral RNA genome with various
136 binding affinities (4-7); however, it has yet to be examined whether coronavirus N
137 protein is able to bind to the poly(A) tail, a common structure in coronavirus genome,
138 subgenomic mRNAs and cellular mRNA. For this, we first tested whether *Escherichia*
139 *coli*-expressed N protein (~65 kDa, Fig. 1B) binds to the ^{32}P-labeled poly(A) tail
140 using electrophoretic mobility shift assay (EMSA). As shown in Fig. 1C, N protein
141 bound to the ^{32}P-labeled 65-nt poly(A) tail (lane 2). In addition, non-radiolabeled
142 competitor 65-nt poly(A) tail was able to compete for this binding by N protein in a
143 dose-dependent manner (lanes 3-5). Conversely, similar results were not found for the
144 binding between N protein and yeast tRNA (lanes 6) or between
145 glutathione *S*-transferase (GST) and ^{32}P-labeled 65-nt poly(A) tail (data not shown).
146 The data suggest that coronavirus N protein is able to bind to the poly(A) tail.
147 As it is well characterized that PABP binds to poly(A) tails with high affinity, we
148 postulated that the potential significance of the poly(A)-binding activity of N protein
149 may be further emphasized if its binding affinity is similar to that of PABP. For this,
150 increasing concentrations of N protein and PABP were separately incubated
151 with ^{32}P-labeled 65-nt poly(A) tail and then analyzed by EMSA. The percentage of
152 bound RNA was then used to derive the dissociation constant (K_d) using the Hill
153 equation and K_d was calculated to be 28.4±3.9 and 17.8±1.2 nM for N protein and
154 PABP (Figs. 1D and 1E), respectively, suggesting that N protein and PABP have
155 similar binding affinities for the 65-nt poly(A) tail. Because the C-terminal domain
156 (CTD) of N protein is mainly involved in oligomerization (29, 30) and the CTD of

PABP has also been reported to possess homodimerization activity (31), the multiple complexes shown in Figs. 1D and 1E resulting from such protein-protein interaction are not unexpected.

To further characterize the poly(A)-binding activity of N protein, RNA probes with various sequence were synthesized (Fig. 1F). The same RNA probes were also examined for their ability to interact with PABP. The K_d for N protein and PABP with RNA probes containing the BCoV 3'-terminal 55 nts and poly(A) tails of decreasing lengths (55 nts+65A, 55 nts+45A, 55 nts+25A or 55 nts) increased (Fig. 1G, left panel), suggesting that the length of the poly(A) tail is the main factor for increasing the binding efficiency of N protein and PABP to the RNA probes. In addition, the K_d for N protein and PABP with 25-nt poly(A) tail was higher than that with the 65-nt poly(A) tail (Fig. 1G, left panel), further suggesting that N protein is a poly(A)-binding protein. Finally, as shown in Fig. 1G (right panel), K_d for N protein and these non-poly(A) sequences containing various types of nts (BCoV-65nts and β-actin-65nts, respectively, Fig. 1F) was ~4-5-fold higher than that for N and the 65-nt poly(A) tail, suggesting that N protein has greater binding affinity for a poly(A) sequence than a non-poly(A) sequence containing various types of nts. Together, the results further suggest that coronavirus N protein, similar to PABP, binds to poly(A) tail with high affinity.

N protein is able to compete with PABP for binding to the poly(A) tail *in vitro* and in cells. To address the question of whether N protein is able to compete with PABP for binding to the poly(A) tail in an environment in which they co-exist *in vitro*, the ^{32}P-labeled poly(A) tail RNA probe was incubated with mixtures containing various molar ratios of N protein to PABP, followed by EMSA. The EMSA results of N protein or PABP binding to the poly(A) tail and the relative binding percentage are

illustrated in the upper and lower panels of Fig. 2A, respectively. As shown in Fig. 2A, upper panel, at molar ratios of N/PABP from 65.6 to 5.7 in lanes 3-7 (with the increase of PABP), a minor (complex 1, indicated by white dot in lane 3) and a major (indicated by white asterisk in lane 3) RNA-protein complex were observed. Since the major complexes in lanes 3-7 corresponded to N-RNA complex in lane 2, the preferential binding of 65-nts poly(A) tail to N protein was determined at molar ratios between 5.7-65.6. With further increase of PABP (i.e., decreased molar ratio of N/PABP from 4.0 to 1.9 in lanes 8-10), the minor complex (complex 1, indicated by white dot in lane 3) in lanes 3-7 became major complex in lanes 8-10, suggesting that the major complex (complex 1) consists of PABP and 65-nts poly(A) tail. Furthermore, with the increase of PABP in lanes 11-13, the complex 1 almost disappeared; however, complex 2 appeared, which corresponded to PABP-RNA complex in lane 14. Together, since the major complex in lanes 8-13 consists of PABP and 65-nts poly(A) tail, the preferential binding of 65-nts poly(A) tail to PABP was determined at molar ratios between 0.6-4.0 (lanes 8-13). Note that a small amount of N protein (~15%, Fig. 2A, lower panel) still bound to the poly(A) tail when the molar ratio of N protein to PABP was from 3.0 to 4.0 (lanes 8 and 9). Based on these results, it was concluded that N protein can compete with PABP for binding to the poly(A) tail *in vitro*, even though at the same molar ratio (lane 12), PABP exhibits better binding affinity to poly(A) tails than N protein.

To determine whether N protein is able to bind to poly(A) tail in infected cells, ^{32}P-labeled 65-nt poly(A) tail was transfected into BCoV- or mock-infected cells and UV cross-linked. Cell lysates were collected and an antibody against PABP or N protein was employed to immunoprecipitate PABP or N protein followed by RNase treatment. As shown in Fig. 2B, left panel, antibody against PABP immunoprecipitated a ~70-kDa protein from mock-infected and BCoV-infected cells

(lanes 4 and 5, respectively); however, in Fig. 2B, right panel, antibody against N protein immunoprecipitated a ~50-kDa protein from BCoV-infected cell (lane 5) but not the mock-infected cell (lane 3). The results suggest that, in addition to PABP, N protein is able to bind to the poly(A) tail in infected cells.

Determination of molar ratio of N protein to PABP in subcellular locations at different stages of infection. As shown in Fig. 2A, the molar ratio of N protein to PABP plays a role in poly(A) tail binding preference. In addition, it has been suggested that coronavirus replication can occur in a modified membrane-associated compartment (32). It was therefore speculated that molar ratios in subcellular locations of coronavirus-infected cells at different stages of infection may also be decisive regarding PABP or N protein binding preference for the poly(A) tail. Thus, subcellular fractions of cytosol and membrane were obtained at various time points of infection, and the amounts of N protein and PABP in each cellular fraction according to immunoblotting (Figs. 3A and 3B, upper panel) were quantified based on a standard curve obtained from known amounts of the proteins. As shown in Figs. 3A and 3B, middle and lower panel, the molar ratio of N protein to PABP in both cytosol and membrane was low (~0.4) during the initial infection, but increased (from ~0.4 to ~2.6 in cytosol and from ~0.3 to ~10.5 in membrane) at later infection stages. The results indicate that the amounts of N protein are increased in both cytosol and membrane at the later time points of infection. Thus, based on the results shown in Figs. 2 and 3, we speculate that the poly(A) tail may preferentially bind with PABP during the initial infection but with N protein in the later infection, especially in membrane-associated structures.

BCoV N protein inhibits viral translation both *in vitro* and *in vivo*. Because the

poly(A) tail is able to bind to N protein with high affinity (Fig. 1) and in infected cells (Fig. 2), we hypothesized that such binding may prevent the poly(A) tail on coronavirus RNA from interacting with translation factors, leading to translation inhibition. To test the hypothesis, a BCoV defective interfering (DI) RNA, a surrogate for the coronavirus genome that has been extensively used for studies of coronavirus gene expression (33-37) (Fig. 4A), was engineered to express EGFP; the construct was designated DI-EGFP. For *in vitro* translation analysis, DI-EGFP with the 65-nt poly(A) tail was first incubated with various amounts of N protein (Fig. 4B) for 15 min to allow the binding of N protein to the 65-nt poly(A) tail on DI-EGFP and then added to a rabbit reticulocyte lysate (RRL) for another 90 min. A similar experiment was performed however DI-EGFP was first incubated with PABP or GST. As shown in Fig. 4B, translation of DI-EGFP with a 65-nt poly(A) tail was inhibited with increasing amounts of N protein but not PABP or GST (data not shown). To test whether the inhibition was due to the effect of N protein on the RRL, various amounts of N protein were first incubated with RRL for 60 min, and then DI-EGFP with the 65-nt poly(A) tail was added. The translation efficiency of DI-EGFP, however, was not altered (data not shown), indicating that N protein at these concentrations had no effect on the translation efficiency of RRL. Accordingly, the reduced translation efficiency shown in Fig. 4B was due to the binding of N protein with DI-EGFP but not the effect of N protein on RRL. Furthermore, it has been shown that translation using RRL still occurs with an mRNA lacking a poly(A) tail although the translation efficiency is affected (38). Consequently, we hypothesized that if the decreased translation efficiency was due to the binding of N protein to the poly(A) tail, translation efficiency of poly(A)-deficient DI-EGFP is not altered with increasing amounts of N protein. To test this, poly(A)-deficient DI-EGFP was generated, incubated with various amounts of N protein for 15 min and then added to the RRL.

As shown in Fig. 4C, the translation efficiency was not significantly affected with increasing amounts of N protein, suggesting that the decreased translation in Fig. 4B may be mostly due to the interaction between N protein and poly(A) tail. Taken together, because N protein apparently had no effect on the translation efficiency of RRL (data not shown) and on translation efficiency of poly(A)-deficient DI-EGFP (Fig. 4C), the inhibitory effect of translation shown in Fig. 4B may be attributed to interaction between the poly(A) tail and N protein. Note that after *in vitro* translation in RRL the amounts of DI-EGFP at various concentrations of N protein were not significantly altered, indicating that the stability of DI-EGFP is not a factor affecting the translation efficiency. It was therefore concluded that N protein is able to inhibit viral translation by binding to the viral poly(A) tail *in vitro*.

To further assess whether translation inhibition by N protein also occurs *in vivo*, the N protein or His-β-actin transcript was transfected into HEK-293T cells followed by transfection of DI-EGFP with a 65-nt poly(A) tail (Fig. 4D, left panel) or by infection of BCoV (Fig. 4F, left panel). Cell lysates were harvested and analyzed by immunoblotting to quantitate the translation efficiency of DI-EGFP and coronavirus nsp1 (representing genome expression). As shown in Fig. 4D, right panel and Fig. 4E, inhibition of the DI-EGFP translation was observed in cells transfected with the N protein transcript at 3, 8 and 16 h in comparison with those transfected with the His-β-actin transcript, suggesting that N protein is able to inhibit translation of DI-EGFP *in vivo*. The similar inhibition results were also obtained in cells infected with BCoV (Fig. 4F, right panel and Fig. 4G), suggesting N protein can inhibit translation of coronavirus genome. Note that the levels of DI-EGFP RNA (Fig. 4D) and viral genomic RNA (Fig. 4F) were similar between the groups at the same time point as confirmed by RT-qPCR (data not shown). Therefore, based on the results of the *in vivo* binding of N protein to poly(A) tail (Fig. 2B) and the *in vitro* analyses

shown in Figs. 4B and 4C, the inhibitory effect of N protein on translation of DI-EGFP and BCoV *in vivo* may at least be partly attributable to the binding of N protein to the poly(A) tail on DI-EGFP and BCoV genome.

BCoV N protein modulates translation of host mRNAs both *in vitro* and *in vivo*. To examine whether the binding of N protein to the poly(A) tail of mRNA also inhibits host mRNA translation, a β-actin transcript with 65-nt poly(A) tail was first incubated with N protein to form an N protein-poly(A) complex and then subjected to an *in vitro* translation assay with the RRL. As shown in Fig. 5A, expression of β-actin transcripts was inhibited with increasing amounts of N protein. As with the *in vitro* translation assay for DI-EGFP (Fig. 4), to further determine whether the inhibitory effect was due to the binding of N protein to the poly(A) tail, a poly(A) tail-deficient β-actin transcript was first incubated with various amounts of N protein followed by the assay. However, inhibition was not observed (Fig. 5B), as no significant difference in expression of the poly(A) tail-deficient β-actin transcript was observed with increasing amounts of N protein. These results (Figs. 5A and 5B) suggest that binding of N protein to the poly(A) tail of the β-actin transcript is a major factor leading to translation inhibition.

In addition to individual cellular mRNAs *in vitro*, inhibition of host mRNA translation by N protein was also examined globally in cells. For this, the N protein transcript or His-tagged β-actin transcript was independently transfected into HEK-293T cells for 1 h, after which the cells were incubated for 3 h in the presence or absence of actinomycin D. After addition of actinomycin D, the cells were labeled with [^{35}S]-methionine for 8 h, and equal amounts of cell lysate were analyzed by SDS-PAGE. As shown in the left panel of Figs. 5C and 5D, inhibition of host protein synthesis was not apparent in cells not treated with actinomycin D; however, with

313 actinomycin D treatment, synthesis of host proteins in cells transfected with the N
314 protein transcript was decreased by ~one-third in comparison with that in cells
315 transfected with the His-tagged β-actin transcript or with mock transfected (Fig. 5C,
316 left panel and Fig. 5D, right panel). The fact that the efficiency of N protein inhibition
317 was better in actinomycin D-treated cells than in untreated cells may indicate that in
318 the absence of nascent mRNA synthesis, expressed N protein was involved in
319 interaction with preexisting mRNAs, leading to inhibition of host protein synthesis. In
320 addition, the levels of host mRNA (represented by GAPDH mRNA) were similar (Fig.
321 5C) between the groups treated with actinomycin D as confirmed by RT-qPCR (data
322 not shown) and thus were not affected by the expressed N protein. Thus, it was
323 concluded that in addition to coronaviral RNA, N protein is also able to globally
324 inhibit host mRNA translation, and based on *in vitro* results (Figs. 5A and 5B), such
325 inhibition in cells may at least partly result from the binding of N protein to the
326 poly(A) tail.
327
328 **Interactions among the poly(A) tail, N protein and PABP.** To elucidate the
329 possible mechanism by which interactions among the poly(A) tail, N protein and
330 PABP regulate gene expression, we first determined whether a poly(A) tail is able to
331 interact with both the N protein and PABP using lysates of infected cell. For this, an
332 84-nt biotinylated RNA, consisting of 19 non-poly(A) nts (containing
333 biotin-conjugated uridine) followed by a 65-nt poly(A) tail, was synthesized and
334 incubated with cell lysates followed by a streptavidin pull-down assay and
335 immunoblotting. As shown in Fig. 6A (lane 1), both the N protein and PABP were
336 detected (indicated by asterisks), demonstrating poly(A) tail interaction. To ensure
337 that the detection of the N protein and PABP was in fact due to interaction with the
338 poly(A) tail and not with the 19 non-poly(A) residues, a biotinylated RNA containing

the 19 non-poly(A) nts was also used. However, neither were observed (data not shown) by immunoblotting, confirming that the 65-nt poly(A) tail, and not 19 non-poly(A) nts, can interact with both the N protein and PABP from infected cell lysates. We next addressed whether the N protein is able to directly bind to the PABP by performing a pull-down assay, in which purified His-tagged PABP (Fig. 6B, left panel) was bound to Ni-NTA beads and mixed with purified untagged N protein (Fig. 6B, right panel). As shown in Fig. 6C, untagged N protein (left panel, lane 1) was co-pelleted by His-tagged PABP, suggesting that the N protein can physically bind to the PABP. Finally, we assessed whether the N protein is able to interact with the PABP from infected cell lysates by incubating Ni-NTA beads with His-tagged N protein and infected cell lysates and subjecting the elute to immunoblotting with an antibody against PABP. As shown in Fig. 6D, a signal at ~70 kDa representing the cellular PABP was observed (left panel, lane 1), suggesting that the N protein is able to interact with cellular PABP from infected cell lysates. Consistently, the reciprocal pull-down assay with His-tagged PABP demonstrated that the PABP can interact with the N protein from infected cell lysates (Fig. 6D, right panel, lane 1). To determine whether RNA bridging is essential for such interaction, RNase treatment was included in the pull-down assay. As shown in Fig. 6D, both the PABP (left panel, lane 6) and N protein (right panel, lane 5) were detected, suggesting RNA bridging is not a requirement for the interaction between the two proteins. Taken together, it was concluded that the poly(A) tail can interact with both the N protein and PABP from infected cell lysates. In addition, the N protein is able to physically bind to the PABP *in vitro* and to interact with PABP from infected cell lysates.

Interactions of the poly(A) tail and N protein with translation factor eIF4G and coronavirus replicase protein nsp9. To further examine the role of the poly(A) tail

and N protein in gene regulation, we first determined whether the poly(A) tail is able to interact with eIF4G and nsp9, a coronavirus replicase protein that is associated with polymerase nsp12 (20), is essential for replication (21) and is involved in the initiation of (-)-strand RNA synthesis (22). To this end, the 84-nt biotinylated RNA described above (consisting of 19 non-poly(A) nts followed by 65-nt poly(A) tail) were used in the streptavidin pull-down assay. As shown in Fig. 7A, both eIF4G (left panel, lane 1) and coronavirus nsp9 (right panel, lane 1) were detected by immunoblotting, though they were not observed with the biotinylated RNA containing only the 19 non-poly(A) tail nts (data not shown), suggesting that the 65-nt poly(A) tail is able to interact with eIF4G and coronavirus nsp9 from infected cell lysates. We next performed the pull-down assay with Ni-NTA beads to determine whether the N protein is able to interact with eIF4G in infected cells. In this case, eIF4G was not detected when using infected cell lysates treated with or without RNase (Fig. 7B, lane 1 and lane 7, respectively) but was detected when using mock-infected cell lysates treated with or without RNase (Fig. 7B, lane 2 and lane 8, respectively). To address whether the lack of eIF4G detection was due to the His-tagged N protein being outcompeted by endogenous N in infected cell lysates, a pull-down assay with protein G beads followed by incubation with an antibody against N protein was employed. Indeed, eIF4G was detected in the absence or presence of RNase (Fig. 7C, lane 1 and lane 6, respectively), suggesting that the N protein can interact with eIF4G from infected cell lysates without the assistance of RNA. Our results show that the N protein is able to bind to the poly(A) tail, yet it is possible that at least a portion of the detected coronavirus nsp9 in Fig. 7A is due to its interaction with the N protein. Another pull-down assay was performed to investigate this possibility. As shown in Fig. 7D, lane 2 and lane 7, nsp9 was detected in infected cell lysates in the absence or presence of RNase treatment, respectively, suggesting that the N protein is able to interact with

nsp9 without an RNA bridge. These data suggest that both the poly(A) tail and N protein are able to interact with the translation factor eIF4G and replicase protein nsp9.

Poly(A)-bound N protein interacts efficiently with eIF4G but not eIF4E. To further examine the translation inhibition caused by binding of the N protein to the poly(A) tail, we next assessed whether N can interact with the translation factor eIF4E. For this, a fixed concentration of biotinylated RNA consisting of 19 non-poly(A) nts followed by the 65-nt poly(A) tail was first incubated with increasing amounts of N (2, 4 and 6 μM) and then with mock-infected cell lysates followed by a streptavidin pull-down assay. In this context, the N protein interacted with eIF4G efficiently (Fig. 8A, lanes 4-6, panel 1), whereas the amount of eIF4E detected decreased (Fig. 8A, lanes 4-6, panel 2) with an increase in N protein (Fig. 8A, lanes 4-6, panel 4), suggesting that the poly(A)-bound N protein cannot interact efficiently with eIF4E. Note that the binding efficiency between the aforementioned biotinylated RNA and the input PABP or N protein increased with increasing amounts of input PABP or N protein as confirmed by immunoblotting shown in panels 3 (lanes 1-3) and 4 (lanes 4-6), respectively. With regard to the observed eIF4E (Fig. 8A, lane 4, panel 2), we interpret that the biotinylated poly(A) tail not bound to N, which resulted from insufficient binding of N to the biotinylated poly(A) tail due to the reduced amount of input N protein (2 μM), was still able to bind to PABP and then eIF4G and eIF4E, leading to detection of eIF4E (Fig. 8A, lane 4, panel 2). Accordingly, with an increasing amount of input N protein, the biotinylated poly(A) tail was almost all bound and thus was unable to interact with eIF4E (Fig. 8A, lanes 5-6, panel 2), supporting the above argument.

To further determine whether the poly(A) tail is able to interact with eIF4G,

417 eIF4E and replication factor nsp9 in infected cells, lysates at different time points of
418 coronavirus infection were incubated with a biotinylated RNA consisting of 19
419 non-poly(A) nts followed by the 65-nt poly(A) tail followed by streptavidin pull-down.
420 As shown in Fig. 8B, levels of eIF4G and eIF4E were decreased (lanes 4-6, panels 1
421 and 2, respectively) with increasing N protein (lanes 4-6, panel 4), whereas nsp9 was
422 increased (lanes 4-6, panel 3). These results suggest that in infected cells, the poly(A)
423 tail is able to interact with eIF4G and eIF4E but that the efficiency is decreased with
424 increasing amounts of N protein. Because the N protein can interact with coronaviral
425 replicase proteins (8-14), we speculate that these viral proteins compete with eIF4G
426 for interaction with N in infected cells, which in our assay would lead to reduced
427 detection of eIF4G. This argument is supported by the increased amounts of nsp9
428 detected (Fig. 8B, lanes 4-6, panel 3), which is also able to interact with the N protein
429 (Fig. 7). Furthermore, the amount of eIF4E detected (Fig. 8B, lanes 4-6, panel 2) may
430 be attributed to the input biotinylated poly(A) tail being bound by PABP followed by
431 eIF4G and eIF4E. In line with this argument, the reduced amount of eIF4E detected
432 (Fig. 8B, lanes 4-6, panel 2) may have resulted from the increased level of poly(A)
433 -bound N protein, which, based on the results shown in Fig. 8A, cannot interact with
434 eIF4E. Together, the poor interaction efficiency between the poly(A) -bound N
435 protein and eIF4E (Fig. 8A) and the decreased interaction efficiency between the
436 poly(A) tail and eIF4G and eIF4E in infected cells (Fig. 8B) may explain the results
437 of decreased translation efficiency observed in coronaviruses and host cells (Figs. 4
438 and 5).
439

440 **DISCUSSION**

441 In the present study, we provide evidence for interactions among the poly(A) tail, N
442 protein and PABP both *in vitro* and in infected cells. We also demonstrate that poly(A)

443 tail binding by the N protein inhibits translation of both coronaviral RNA and host
444 mRNA. Further examination revealed that both the poly(A) tail and N protein are able
445 to interact with the translation factor eIF4G and replicase protein nsp9. However, the
446 poly(A)-bound N protein cannot interact efficiently with eIF4E. The mechanism by
447 which the aforementioned interactions regulate gene expression in coronaviruses and
448 host cells and the biological relevance of such interactions are discussed below.
449 It has been demonstrated that the binding of PABP to a poly(A) tail (39)
450 followed by eIF4G and eIF4E binding to form a translation initiation complex is
451 required for efficient protein synthesis. In the current study, we showed that an N
452 protein-bound poly(A) tail can interact with eIF4G but largely cannot interact with
453 eIF4E (Fig. 8). Therefore, such an inefficient interaction may affect the constitution of
454 a stable translation initiation complex, leading to decreased translation efficiency, as
455 shown in Figs. 4 and 5. It is known that eIF4G can bind to eIF4E; however, the
456 mechanism by which the poly(A)-bound N protein is able to interact with eIF4G but
457 not with eIF4E remains to be experimentally elucidated. It has been suggested that
458 allosteric interactions mediated by the poly(A) tail, PABP, eIF4G, and eIF4E are
459 critical for translation initiation (39-41) and that molecules such as 4EGI-1 (42) and
460 eIF4E-binding proteins (4EBPs) (43) are also involved in these interactions. Therefore,
461 it is possible that binding of the N protein to eIF4G may cause a conformational
462 change in eIF4G and thus decrease the binding efficiency with eIF4E. Alternatively,
463 the N protein may use the same binding site as utilized for eIF4E to bind to eIF4G;
464 thus, once eIF4G is bound to the N protein, eIF4G cannot bind to eIF4E, leading to
465 undetectable eIF4E in pull-down assays. These arguments are in agreement with
466 results of an *in vitro* translation assay (Figs. 4B and 5A) in which the poly(A) tail was
467 first bound by the N protein, resulting in decreased translation efficiency. Accordingly,
468 such a mechanism (binding of N to the poly(A) tail) may explain, in part, why

translation was inhibited in cells (Figs. 4D-G and 5C-D). To our knowledge, the translation inhibition caused by the binding of N to the poly(A) tail has not been previously documented for coronaviruses.

Regarding cellular mRNA, as argued above, binding of N to the poly(A) tail can inhibit translation, possibly preventing the use of mRNA for gene expression. Nevertheless, the outcome of such binding may not be applicable to coronavirus genomic RNA and subgenomic mRNA (sgmRNA) because the N protein can interact with viral replicase proteins (8-14) and nsp9 (the current study; Fig. 7). We speculate that, in addition to translation inhibition, N protein binding to the poly(A) tail followed by interaction with replicase protein may be a highly important task for coronavirus RNA species including sgmRNA (44). Thus, further study is required to demonstrate the biological relevance of the interaction. One may argue that the poly(A) tail of cellular mRNA may also be bound by the N protein followed by interaction with these replicase proteins. However, because *cis*-acting elements located at the 5'- and 3'-termini of the coronavirus have been demonstrated to be required for coronavirus replication (45), lack of these elements in cellular mRNA would explain the above argument.

According to the elegant model proposed by Hurst et al. (10), after release of an N protein-bound viral genome into the cell, displacement of the N protein from the 5' two-thirds of the genome may allow replicase proteins to be translated, including nsp3. This translated nsp3 then associates with infecting (residual) N protein, which is bound to the 3' end of the incoming viral genome, and tethers the complex to the endoplasmic reticulum (ER). Based on the results of the current study, we propose a modification of this model with more details, as follows. Because coronavirus assembly occurs at the membrane (13), where the N protein concentration is higher than that of PABP (Fig. 3), we speculate that the incoming viral genomic poly(A) tail

may be bound by N protein. Additionally, because N has higher binding affinity for the poly(A) tail than for a non-poly(A) sequence (Fig. 1), it is possible that for the incoming viral genomic RNA, the N protein disassociates from all genome regions except the poly(A) tail, allowing translation of replicase proteins to occur. At this point, it can be expected that the translation efficiency may be decreased because the poly(A) tail is bound by N (Fig. 4). However, once nsp3 is synthesized, it can associate with the N protein and tether the N-poly(A)-bound genome to the replication complex at the ER (9, 10) for the first round of replication to synthesize a nascent genomic RNA and sgmRNA.

During infection, the genome of the positive-sense RNA virus functions as a template for both translation and replication; therefore, these two processes must be regulated to enable efficient gene expression. In coronaviruses, however, the mechanisms by which the two processes are regulated remain unclear. Based on the results from the current study and others, (i) the poly(A) tail can be bound by PABP and function in translation (46); (ii) the poly(A) tail is a start site for (-)-strand RNA synthesis (47); (iii) the poly(A) tail can also be bound by the N protein with high affinity (Fig. 1); (iv) the N protein can interact with viral replicase proteins (8-14) and nsp9 (Fig. 5) and participates in replication (15-18); and (v) nsp9 is required for coronavirus replication (21) and is associated with the replication complex for (-)-strand initiation according to the model proposed by Züst et al. (22). Altogether, we speculate that similar to the 5'-terminal cloverleaf in polioviruses (27, 28), the coronavirus 3'-poly(A) tail, which is required for both translation and replication (36, 46), may function as a regulator to coordinate utilization of the genome for translation (binding to PABP) or replication (binding to N). Further experiments are required to demonstrated whether binding of the poly(A) tail to N protein is a key step needed to regulate the two processes.

521 Based on the data presented herein and reported by others, a mechanism by
522 which interactions among the poly(A) tail, PABP and N protein regulate gene
523 expression in coronaviruses is proposed, as illustrated in Fig. 9. At the early stage of
524 infection, PABP is abundant (Fig. 3). The poly(A) tail of the coronavirus genomic
525 RNA may predominantly be bound by PABP followed by interaction with other
526 translation factors such as eIF4G and eIF4E (Fig. 8), leading to translation. With an
527 increase in N protein in the later stage of infection (Fig. 3), binding of the N protein to
528 poly(A) tails on coronavirus genomic RNA decreases the interaction efficiency
529 between the poly(A) tail and translation factors such as eIF4E (Fig. 8), leading to
530 translation inhibition.

531 Although we understand that additional data are required to determine the role of
532 binding of the poly(A) tail to N protein in the switch from genome translation to
533 replication, we attempt to explain the potential gene regulation in coronaviruses based
534 on the current findings with different viewpoints. First, in terms of an individual viral
535 genomic RNA, binding of the poly(A) tail by PABP or the N protein may decide the
536 subsequent function of the RNA. Second, in terms of the infection stage, the major
537 proportion of viral RNA in the early stage of infection functions in translation via
538 binding of the poly(A) tail by PABP, whereas in later stages, binding of the poly(A)
539 tail by the N protein and subsequent replicase proteins downregulates translation and
540 may lead to replication. Third, in terms of subcellular location, the N protein has been
541 shown to accumulate at a modified membrane-associated compartment where
542 coronavirus replication and assembly occur (32, 48). Thus, the findings of the study
543 reporting that membrane levels of PABP are much reduced compared to the cytosolic
544 fraction (49) support our results that a high molar ratio of N to PABP was detected in
545 the membrane fraction (Fig. 3), leading to binding of the poly(A) by the N protein and
546 possibly thereby directing the viral RNA toward replication. In addition, we argue that

the aforementioned interactions and their effects on the regulation of gene expression are stochastic, rather than an all-or-none process in the infected cells.

In conclusion, we demonstrate interactions among the poly(A) tail, N protein and PABP, as well as those among the N protein and eIF4G and nsp9. Of the interactions shown in this study, binding of the poly(A) tail to PABP followed by eIF4G and eIF4E leads to translation. However, binding of poly(A) tail to N protein decreases the interaction efficiency between the poly(A) tail and eIF4E, leading to translation inhibition. In addition, whether binding of the poly(A) tail by the N protein followed by interaction with nsp9 may further direct viral RNA toward (-)-strand RNA synthesis remains to be determined.

MATERIALS AND METHODS

Viruses, cells and antibodies. Human rectum tumor (HRT)-18 and HEK-293T cells were obtained from David A. Brian (University of Tennessee, TN) and maintained in Dulbecco's modified Eagle's medium (DMEM) supplemented with 10% fetal bovine serum (FBS) (HyClone) and antibiotics at 37°C with 5% CO_2. The plaque-purified Mebus strain of BCoV (GenBank accession no. U00735) was grown on an HRT-18 cell line as described (50, 51). Anti-N protein (BCoV) antibody and anti-nsp9 (BCoV) antibody were obtained from David A. Brian (University of Tennessee, TN). Antibodies used for this study are as follows: anti-EGFP antibody (GeneTex), anti-PABP antibody (Cell Signaling Technology), anti-eIF4G antibody (Cell Signaling Technology), anti-eIF4E antibody (Cell Signaling Technology), anti-GAPDH antibody (GeneTex), anti-calnexin antibody (Cell Signaling Technology) and anti-His-tag antibody (Bio-Rad).

572

573 **Construction of plasmids and DNA templates for RNA probes.** The DNA
574 templates 55nts+65A, 55nts, 65A, 55nts+45A, 55nts+25A, 25A, and BCoV-65nts
575 for synthesis of RNA probes were produced by PCR. The template for the 65A
576 and 25A containing 65 and 25 adenosine residues were generated by PCR using a
577 primer containing 65 and 25 thymidine nucleotides, respectively, and a primer
578 containing T7 promoter sequence plus 3 guanosine residues. Therefore, except
579 for 3 guanosine residues, there is no extra non-adenosine residues in both RNA
580 probes after *in vitro* transcription. To synthesize a DNA template containing the
581 65-nt poly(A) tail and 19 non-poly(A) tail, a primer with sequence of
582 5'-TGTAATACGACTCACTATAGGGCCAATTGAAGAAT-3' and a primer with
583 sequence of 5'-T(65) GTGATTCTTCAATTGG-3' were used for PCR. Constructs
584 actin-65nts for the RNA probe and His-tagged β-actin for *in vitro* translation
585 were amplified by RT-PCR using RNA extracted from HRT-18 cells. To construct
586 DI-EGFP, EGFP gene was inserted into BCoV DI RNA at the site between ORF
587 1a and N protein gene. For this, a DNA fragment containing the EGFP sequence
588 and *Hpa*I and *Xba*I restriction enzyme sites was amplified by an overlap PCR
589 mutagenesis procedure, digested with *Hpa*I and *Xba*I and ligated into *Hpa*I and
590 *Xba*I-linearized pDrepI to create pDI-EGFP. The resulting pDI-EGFP contained
591 full-length EGFP and N protein gene.

592

593 **Expression of recombinant proteins.** For His-tagged N protein, pET32aN,
594 which contains BCoV N protein gene, was transformed into *Escherichia coli*

595 BL21 (DE3) cells followed by inoculating into LB medium. The cells were then
596 induced with isopropyl thio-β-D-galactoside, harvested by centrifugation and
597 resuspended in PBS and then sonicated. The supernatant containing the
598 recombinant protein was purified through the 6xHis tag by immobilized metal ion
599 affinity chromatography with EDTA-resistant Ni Sepharose excel resin (GE
600 Healthcare) and loaded on a nickel-chelating column (GE Healthcare). Fractions
601 containing N protein were dialyzed and collected. Because the expressed BCoV
602 N protein also contains His-, Trx- and S-Tag coding sequences, the resulting
603 molecular weight is estimated to be ~65 kDa. To obtain N protein without the
604 His-tag, the tag along with Trx- and S-Tag was removed using PreScission
605 protease (GE Healthcare). To purify His-tagged PABP, pET28aPABP, which
606 contains PABP gene (GenBank accession no. NM_002568), was transformed into
607 *E. coli* BL21 (DE3) pLysS cells and the following procedures were similar to
608 those for expression of N protein as described above.
609
610 **Electrophoretic mobility shift assay (EMSA) and dissociation constant (K_d).**
611 An *in vitro* transcription reaction for synthesizing ^{32}P-labeled RNA for EMSA
612 was carried out using T7 RNA polymerase and [α-^{32}P]ATP as specified by the
613 manufacturer (Promega). To purify ^{32}P-labeled RNA, the synthesized ^{32}P-labeled
614 RNA was separated on 6% sequencing gels, and passive elution was performed
615 followed by phenol/chloroform extraction. The ^{32}P-labeled RNA and N protein
616 were added to the binding reaction containing 20 mM HEPES (pH 7.5), 6 mM
617 $MgCl_2$, 1.5 μM EGTA, 22.5 mM NaCl, 330 mM KCl, 36% glycerol, 3.6 mM

DTT, 82.5 µg/ ml BSA, and 36% glycerol and incubated for 15 min at 37°C with 1 U/ml RNasin (Promega) (final concentration for ^{32}P-labeled RNA and N protein is 1 nM and 5 nM, respectively). Reactions with unlabeled competitor at 1-, 10- and 100-fold excess and non-specific yeast tRNA (0.1 mg/mL) were also performed in parallel. The RNA-protein complexes were resolved on a native polyacrylamide gel in TBE buffer (50 mM Tris, 45 mM boric acid, 0.5 mM EDTA) at constant voltage at room temperature, dried, and analyzed by autoradiography. To determine the binding affinity, a fixed concentration of 0.2 nM ^{32}P -labeled RNA was titrated with protein (0, 14, 71, 143, 286, 533 nM), and the bound RNA-protein complexes were separated from unbound RNA using an 8% polyacrylamide gel. Free and bound RNA were quantitated and fit to the Hill equation: RNA bound= b*[P]n/(Kd^n +$[P]^n$), where b is the upper binding limit, [P] is the protein concentration, n is the Hill coefficient and K_d is the dissociation constant. GraphPad Prism was used. K_d was calculated based on at least three independent experiments.

UV cross-linking of RNA to N protein. HEK-293T cells were mock-infected or infected with BCoV. After 16 h of infection, ^{32}P-labeled 65-nt poly(A) tail was transfected using Lipofectamine 2000 (Thermo Fisher Scientific) according to the manufacturer's instruction and at 2 h posttransfection cells were washed by phosphate-buffered saline (PBS). Cells were subjected to irradiation on ice for 5 min at 254 nm with ~4000 µwatts/cm^2 using a Spectrolinker (XL-1000, Spectrolinker^{TM}). Cell lysates were collected and treated with RNase mix

containig10mM Tris (pH 7.5), 400 U/ml micrococcal nuclease, 1mM $CaCl_2$, 1% aprotinin, 2 mg/ml leupeptin/pepstatin, 100mM PMSF, 0.1 mg/ml RNase A and RNase T1) at 37°C for 30 min. RNase-treated samples were centrifuged and supernatants were collected and pre-cleared for 1 h at 4°C by incubation with protein G beads (MagQu). The beads were then removed and immunoprecipitaed with an antibody against N protein at 4°C overnight followed by incubation with protein G beads for 4 h at 4°C using tilt rotation. After extensive washing, the RNA-protein complexes were resuspended in SDS-PAGE loading dye, resolved by SDS-PAGE, dried and visualized by autoradiography.

Immunoprecipitation and pull-down assay. His-tagged PABP (25 µg) was mixed with N protein in 100 µl binding buffer containing 50 mM sodium phosphate (pH 7.4), 300 mM NaCl, and 0.02% Tween 20, and Qbeads-NTA-Ni (MagQu) were added. The mixture was incubated with tilt rotation for 30 min at room temperature. The beads were washed 3 times with 1 ml binding buffer containing 50 mM sodium phosphate (pH 7.4), 300 mM NaCl, and 0.02% Tween 20. Proteins bound to the beads were eluted in SDS sample buffer, resolved by SDS-PAGE and analyzed by western blotting. The same method was employed to analyze proteins from cell lysates interacting with His-tagged N protein or His-tagged PABP in the presence or absence of RNase mix. Immunoprecipitation assay with N antibody bound to the protein G-coated magnetic beads followed by incubation with infected cell lysates was performed according to the manufacturer's instructions (MagQu). Proteins bound to the beads were

analyzed by immunoblotting with antibody against eIF4G.

Biotinylated RNA pull-down assays. To synthesize RNA labeled with biotin, the DNA template containing the 65-nt poly(A) tail and 19 non-poly(A) tail nts or only 19 non-poly(A) tail nts was used for *in vitro* transcription with T7 polymerase (Promega) in the presence of a biotin-UTP labeling NTP mixture (Roche), as recommended by the manufacturer. After purification, biotinylated RNA was incubated with cell lysates in TE buffer. After incubation at room temperature for 30 min, a streptavidin suspension (MagQu) was added to the mixture and incubated for 30 min at room temperature followed by three washes with binding buffer. The protein-associated beads were boiled with SDS-PAGE loading buffer for 5 min and analyzed by immunoblotting.

***In vitro* and *in vivo* translation assays.** Capped transcripts for *in vitro* translation were prepared using the T7 mMessage mMachine kit (Ambion), according to the manufacturer's protocol. For the *in vitro* translation assay, 1 μg of capped transcript was added to a mixture containing 17.5 μl rabbit reticulocyte lysate (RRL) (Promega), 20 U RNasin RNase inhibitor (Promega), 1 μl amino acid mixture minus methionine and 20 μCi [^{35}S]-methionine. After incubation at 30°C for 1 h, the samples were resolved by 10% SDS-PAGE. The gel was then dried and exposed to Kodak XAR-5 film. The films were scanned and quantified with ImageJ software (NIH, Bethesda, MD). For a loading control, 1 μg of each capped transcript was resolved on a formaldehyde-agarose gel and stained with

687 ethidium bromide, followed by band density quantitation using ImageJ software
688 (NIH, Bethesda, MD). For the effect of N protein on translation of DI-EGFP *in*
689 *vivo*, HEK-293T cells were independently transfected with 3 μg of N protein or
690 the His-tagged β-actin transcript using Lipofectamine 2000 (Thermo
691 Fisher Scientific) according to the manufacturer's instruction. After 8 h of
692 transfection, HEK-293T cells were transfected with 3 μg of DI-EGFP. Cell
693 lysates were collected after 3, 8 and 16 h and equivalent amounts of cell lysates
694 were analyzed by immunoblotting. The amounts of translated products were
695 normalized with loading control GAPDH and the amounts of DI-EGFP RNA
696 quantified by RT-qPCR. For the effect of N protein on coronavirus translation *in*
697 *vivo*, HEK-293T cells were independently transfected with 3 μg of N protein or
698 the His-tagged β-actin transcript. After 8 h of transfection, HEK-293T cells were
699 infected with BCoV. Cell lysates were collected at the time of postinfection as
700 indicated in Fig. 4F and equivalent amounts of cell lysates were analyzed by
701 immunoblotting. The amounts of translated products were also normalized with
702 loading control GAPDH and the amounts of BCoV genomic RNA quantified by
703 RT-qPCR. For the effect of N protein on host protein synthesis, HEK-293T cells
704 were mock transfected or independently transfected with N protein or the
705 His-β-actin transcript. After 1 h, HEK-293T cells were incubated in medium in
706 the presence or absence of actinomycin D (Thermo Fisher Scientific) for 8 h and
707 incubated with methionine-free medium for 30 min followed by 20 μCi of
708 [^{35}S]-methionine for 1 h. The cells were then collected and equivalent amounts of
709 cell lysates were analyzed by SDS-PAGE gel. The gel was exposed to X-ray film

or Coomassie blue-stained followed by the quantification with ImageJ software (NIH, Bethesda, MD). The amounts of [^{35}S]-methionine-labeled host proteins were then normalized with the amounts of Coomassie blue-stained proteins and GAPDH mRNA quantified by RT-qPCR.

Statistical analysis. Student's unpaired t test was used for statistical analysis of the data using Prism 6.0 software (GraphPad Software, Inc.). The values in the study are presented as the mean ± SD (n = 3); *p<0.05, **p<0.01 and ***p<0.001.

ACKNOWLEDGEMENTS

We thank Dr. Wei-Li Hsu at National Chung Hsing University, Taiwan, for the assistance of RNA-protein interaction experiment and Dr. Chih-Jung Kuo at National Chung Hsing University, Taiwan, for the help of protein purification. We also would like to dedicate the work to Dr. David A. Brian (1941-2014), University of Tennessee, and thank him for many helpful discussions in the initial stage of the work.

REFERENCES

1. International Committee on Taxonomy of Viruses., King AMQ. 2012. Virus taxonomy : classification and nomenclature of viruses : ninth report of the International Committee on Taxonomy of Viruses. Academic Press, London ; Waltham, MA.
2. Lee S, Lee C. 2014. Complete Genome Characterization of Korean Porcine Deltacoronavirus Strain KOR/KNU14-04/2014. Genome Announc 2.
3. Masters PS. 2006. The molecular biology of coronaviruses. Adv Virus Res 66:193-292.
4. Chen H, Gill A, Dove BK, Emmett SR, Kemp CF, Ritchie MA, Dee M,

Hiscox JA. 2005. Mass spectroscopic characterization of the coronavirus infectious bronchitis virus nucleoprotein and elucidation of the role of phosphorylation in RNA binding by using surface plasmon resonance. J Virol 79:1164-79.

5. Nelson GW, Stohlman SA. 1993. Localization of the RNA-binding domain of mouse hepatitis virus nucleocapsid protein. J Gen Virol 74 (Pt 9):1975-9.

6. Cologna R, Spagnolo JF, Hogue BG. 2000. Identification of nucleocapsid binding sites within coronavirus-defective genomes. Virology 277:235-249.

7. Grossoehme NE, Li LC, Keane SC, Liu PH, Dann CE, Leibowitz JL, Giedroc DP. 2009. Coronavirus N Protein N-Terminal Domain (NTD) Specifically Binds the Transcriptional Regulatory Sequence (TRS) and Melts TRS-cTRS RNA Duplexes. Journal of Molecular Biology 394:544-557.

8. Verheije MH, Hagemeijer MC, Ulasli M, Reggiori F, Rottier PJM, Masters PS, de Haan CAM. 2010. The Coronavirus Nucleocapsid Protein Is Dynamically Associated with the Replication-Transcription Complexes. Journal of Virology 84:11575-11579.

9. Hurst KR, Ye R, Goebel SJ, Jayaraman P, Masters PS. 2010. An Interaction between the Nucleocapsid Protein and a Component of the Replicase-Transcriptase Complex Is Crucial for the Infectivity of Coronavirus Genomic RNA. Journal of Virology 84:10276-10288.

10. Hurst KR, Koetzner CA, Masters PS. 2013. Characterization of a Critical Interaction between the Coronavirus Nucleocapsid Protein and Nonstructural Protein 3 of the Viral Replicase-Transcriptase Complex. Journal of Virology 87:9159-9172.

11. Denison MR, Spaan WJM, van der Meer Y, Gibson CA, Sims AC, Prentice E, Lu XT. 1999. The putative helicase of the coronavirus mouse hepatitis virus is processed from the replicase gene polyprotein and localizes in complexes that are active in viral RNA synthesis. Journal of Virology 73:6862-6871.

12. Sims AC, Ostermann J, Denison MR. 2000. Mouse hepatitis virus replicase proteins associate with two distinct populations of intracellular membranes. Journal of Virology 74:5647-5654.

13. Stertz S, Reichelt M, Spiegel M, Kuri T, Martinez-Sobrido L, Garcia-Sastre A, Weber F, Kochs G. 2007. The intracellular sites of early replication and budding of SARS-coronavirus. Virology 361:304-315.

14. van der Meer Y, Snijder EJ, Dobbe JC, Schleich S, Denison MR, Spaan WJM, Locker JK. 1999. Localization of mouse hepatitis virus nonstructural proteins and RNA synthesis indicates a role for late endosomes in viral replication. Journal of Virology 73:7641-7657.

15. Chang RY, Brian DA. 1996. cis requirement for N-specific protein sequence in bovine coronavirus defective interfering RNA replication. Journal of Virology 70:2201-2207.
16. Yount B, Denison MR, Weiss SR, Baric RS. 2002. Systematic assembly of a full-length infectious cDNA of mouse hepatitis virus strain A59. Journal of Virology 76:11065-11078.
17. Almazan F, Galan C, Enjuanes L. 2004. The nucleoprotein is required for efficient coronavirus genome replication. J Virol 78:12683-8.
18. Schelle B, Karl N, Ludewig B, Siddell SG, Thiel V. 2005. Selective replication of coronavirus genomes that express nucleocapsid protein. J Virol 79:6620-30.
19. Wu CH, Chen PJ, Yeh SH. 2014. Nucleocapsid phosphorylation and RNA helicase DDX1 recruitment enables coronavirus transition from discontinuous to continuous transcription. Cell Host Microbe 16:462-72.
20. Brockway SM, Clay CT, Lu XT, Denison MR. 2003. Characterization of the expression, intracellular localization, and replication complex association of the putative mouse hepatitis virus RNA-dependent RNA polymerase. Journal of Virology 77:10515-10527.
21. Miknis ZJ, Donaldson EF, Umland TC, Rimmer RA, Baric RS, Schultz LW. 2009. Severe Acute Respiratory Syndrome Coronavirus nsp9 Dimerization Is Essential for Efficient Viral Growth. Journal of Virology 83:3007-3018.
22. Zust R, Miller TB, Goebel SJ, Thiel V, Masters PS. 2008. Genetic interactions between an essential 3 ' cis-acting RNA pseudoknot, replicase gene products, and the extreme 3 ' end of the mouse coronavirus genome. Journal of Virology 82:1214-1228.
23. Deo RC, Bonanno JB, Sonenberg N, Burley SK. 1999. Recognition of polyadenylate RNA by the poly(A)-binding protein. Cell 98:835-45.
24. Gorgoni B, Gray NK. 2004. The roles of cytoplasmic poly(A)-binding proteins in regulating gene expression: a developmental perspective. Brief Funct Genomic Proteomic 3:125-41.
25. Gingras AC, Raught B, Sonenberg N. 1999. eIF4 initiation factors: effectors of mRNA recruitment to ribosomes and regulators of translation. Annu Rev Biochem 68:913-63.
26. Merrick WC. 2004. Cap-dependent and cap-independent translation in eukaryotic systems. Gene 332:1-11.
27. Gamarnik AV, Andino R. 1998. Switch from translation to RNA replication in a positive-stranded RNA virus. Genes Dev 12:2293-304.
28. Barton DJ, Morasco BJ, Flanegan JB. 1999. Translating ribosomes inhibit poliovirus negative-strand RNA synthesis. J Virol 73:10104-12.

29. Yu IM, Gustafson CLT, Diao JB, Burgner JW, Li ZH, Zhang JQ, Chen J. 2005. Recombinant severe acute respiratory syndrome (SARS) coronavirus nucleocapsid protein forms a dimer through its c-terminal domain. Journal of Biological Chemistry 280:23280-23286.
30. Lo YS, Lin SY, Wang SM, Wang CT, Chiu YL, Huang TH, Hou MH. 2013. Oligomerization of the carboxyl terminal domain of the human coronavirus 229E nucleocapsid protein. Febs Letters 587:120-127.
31. Kuhn U, Pieler T. 1996. Xenopus poly(A) binding protein: Functional domains in RNA binding and protein-protein interaction. Journal of Molecular Biology 256:20-30.
32. Knoops K, Kikkert M, van den Worm SHE, Zevenhoven-Dobbe JC, van der Meer Y, Koster AJ, Mommaas AM, Snijder EJ. 2008. SARS-coronavirus replication is supported by a reticulovesicular network of modified endoplasmic reticulum. Plos Biology 6:1957-1974.
33. Brown CG, Nixon KS, Senanayake SD, Brian DA. 2007. An RNA stem-loop within the bovine coronavirus nsp1 coding region is a cis-acting element in defective interfering RNA replication. J Virol 81:7716-24.
34. Chang RY, Hofmann MA, Sethna PB, Brian DA. 1994. A cis-acting function for the coronavirus leader in defective interfering RNA replication. J Virol 68:8223-31.
35. Raman S, Brian DA. 2005. Stem-loop IV in the 5' untranslated region is a cis-acting element in bovine coronavirus defective interfering RNA replication. J Virol 79:12434-46.
36. Spagnolo JF, Hogue BG. 2000. Host protein interactions with the 3' end of bovine coronavirus RNA and the requirement of the poly(A) tail for coronavirus defective genome replication. J Virol 74:5053-65.
37. Wu HY, Brian DA. 2007. 5'-proximal hot spot for an inducible positive-to-negative-strand template switch by coronavirus RNA-dependent RNA polymerase. J Virol 81:3206-15.
38. Soto Rifo R, Ricci EP, Decimo D, Moncorge O, Ohlmann T. 2007. Back to basics: the untreated rabbit reticulocyte lysate as a competitive system to recapitulate cap/poly(A) synergy and the selective advantage of IRES-driven translation. Nucleic Acids Research 35.
39. Hong KY, Lee SH, Gu S, Kim E, An S, Kwon J, Lee JB, Jang SK. 2017. The bent conformation of poly(A)-binding protein induced by RNA-binding is required for its translational activation function. Rna Biology 14:370-377.
40. Gross JD, Moerke NJ, von der Haar T, Lugovskoy AA, Sachs AB, McCarthy JE, Wagner G. 2003. Ribosome loading onto the mRNA cap is driven by

conformational coupling between eIF4G and eIF4E. Cell 115:739-50.
41. Prevot D, Darlix JL, Ohlmann T. 2003. Conducting the initiation of protein synthesis: the role of eIF4G. Biol Cell 95:141-56.
42. Papadopoulos E, Jenni S, Kabha E, Takrouri KJ, Yi T, Salvi N, Luna RE, Gavathiotis E, Mahalingam P, Arthanari H, Rodriguez-Mias R, Yefidoff-Freedman R, Aktas BH, Chorev M, Halperin JA, Wagner G. 2014. Structure of the eukaryotic translation initiation factor eIF4E in complex with 4EGI-1 reveals an allosteric mechanism for dissociating eIF4G. Proc Natl Acad Sci U S A 111:E3187-95.
43. Gingras AC, Raught B, Gygi SP, Niedzwiecka A, Miron M, Burley SK, Polakiewicz RD, Wyslouch-Cieszynska A, Aebersold R, Sonenberg N. 2001. Hierarchical phosphorylation of the translation inhibitor 4E-BP1. Genes Dev 15:2852-64.
44. Wu HY, Brian DA. 2010. Subgenomic messenger RNA amplification in coronaviruses. Proc Natl Acad Sci U S A 107:12257-62.
45. Madhugiri R, Fricke M, Marz M, Ziebuhr J. 2016. Coronavirus cis-Acting RNA Elements. Advances in Virus Research, Vol 96: Coronaviruses 96:127-163.
46. Wu HY, Ke TY, Liao WY, Chang NY. 2013. Regulation of Coronaviral Poly(A) Tail Length during Infection. PLoS One 8:e70548.
47. Hofmann MA, Brian DA. 1991. The 5' End of Coronavirus Minus-Strand Rnas Contains a Short Poly(U) Tract. Journal of Virology 65:6331-6333.
48. Bost AG, Prentice E, Denison MR. 2001. Mouse hepatitis virus replicase protein complexes are translocated to sites of M protein accumulation in the ERGIC at late times of infection. Virology 285:21-29.
49. Lerner RS, Nicchitta CV. 2006. mRNA translation is compartmentalized to the endoplasmic reticulum following physiological inhibition of cap-dependent translation. Rna-a Publication of the Rna Society 12:775-789.
50. King B, Brian DA. 1982. Bovine coronavirus structural proteins. J Virol 42:700-7.
51. Lapps W, Hogue BG, Brian DA. 1987. Sequence analysis of the bovine coronavirus nucleocapsid and matrix protein genes. Virology 157:47-57.

FIGURE LEGENDS

Fig. 1. Coronavirus N protein binds to poly(A) tail with high affinity. (A) Schematic diagram showing the position of the poly(A) tail in the coronavirus

genome. (B) *E. coli*-expressed coronavirus N protein (~65 kDa) stained with Coomassie blue (left panel) or analyzed by immunoblotting (right panel). (C) EMSA showing the binding specificity of the 65-nt poly(A) tail with N protein. Unlabeled competitor was at 1-, 10- and 100-fold excess and non-specific yeast tRNA (0.1 mg/mL) were also performed. (D) and (E) Upper panel: EMSA showing binding experiments using a fixed concentration of ^{32}P-labeled 65-nt poly(A) tail with increasing amounts (0, 14, 71, 143, 286, 533 nM) of N protein (D) or PABP (E). Complexes 1-4 in (D) were predicted to consist of 1-4 N proteins, respectively, and ^{32}P-labeled 65-nt poly(A) tail, while complexes 1-4 in (E) were predicted to consist of 1-4 PABPs, respectively, and ^{32}P-labeled 65-nt poly(A) tail. Lower panel: a plot of a fraction of bound RNA against the protein concentration is presented for the gel in the upper panel and fits the Hill equation for K_d determination. (F) RNA probes used for determination of the binding affinity with N protein and PABP. (G) The K_d value of RNA probes illustrated in (F) with N protein and PABP. Values in (D), (E) and (G) represent the mean±SD (n=3) of three independent experiments.

Fig. 2. N protein competes with PABP for binding to the poly(A) tail. (A) Upper panel: *in vitro* analysis for preferential binding of the ^{32}P-labeled 65-nt poly(A) tail in an environment containing various molar ratios of N protein to PABP by EMSA (lanes 2-14). Lane 1: ^{32}P-labeled RNA only. Gels were spliced for labeling purposes. Lower panel: the relative binding percentage of N protein and PABP with the poly(A) tail was determined according to the results shown in the upper panel. (B) Identification of the binding of PABP and N protein with poly(A) tail *in vivo*. The ^{32}P-labeled 65-nt poly(A) tail was transfected into cells followed by UV cross-linking and immunoprecipitation using an anti-PABP (left panel) or anti-N protein (right panel) antibody. The resulting products were analyzed by SDS-PAGE and autoradiographed.

Values in (A) represent the mean±SD (n=3) of three independent experiments.

Fig. 3. Molar ratio of N protein to PABP in subcellular fractions during infection. (A-B) Upper panel: N protein and PABP immunobloting analysis for the cytosol (A) or membrane (B). Middle and lower panel: molar ratio of N protein to PABP and relative percentage between N protein and PABP, respectively. The amounts of N protein and PABP were measured as follows. Different known concentrations of N protein and PABP were identified by immunobloting using antibodies against both N protein and PABP. The signals were scanned densitometrically and then plotted against the concentration to obtain a standard curve for the quantitation of N protein and PABP shown in upper panel. Values in (A) and (B) represent the mean±SD (n=3) of three independent experiments. hpi, hour postinfection.

Fig. 4. Translation inhibition of coronaviral RNA by N protein. (A) Diagram of the BCoV genome, BCoV DI RNA and its derivative DI-EGFP. DI-EGFP was employed for the following translation analyses. (B) Left panel: *in vitro*-synthesized fusion protein (top) from 1 μg of input DI-EGFP RNA transcript with the 65-nt poly(A) tail (Ipt. DI.) (middle), which was preincubated first with 0, 2 and 4 μM of N protein (bottom) and then subjected to *in vitro* translation in RRL. Right panel: relative levels of *in vitro*-synthesized DI-EGFP fusion protein. The values shown are relative to the amount of synthesis in the absence of N protein (i.e., 0 μM of N protein). (C) Left panel: *in vitro*-synthesized fusion protein (top) from 1 μg of input poly(A) tail-deficient DI-EGFP RNA transcript (Ipt. DI.) (middle), which was preincubated with 0, 2 and 4 μM of N protein (bottom) and then subjected to *in vitro* translation in RRL. Right panel: relative levels of *in vitro*-synthesized DI-EGFP fusion protein. The values shown are relative to the amount of synthesis in the

absence of N protein (i.e., 0 μM of N protein). (D) Left panel: diagram showing the experimental procedures to determine the effect of N protein on the translation efficiency of DI-EGFP (with 65-nt poly(A) tail) *in vivo*. Right panel: immunoblotting showing the synthesis of the fusion protein from DI-EGFP in the presence of N protein or His-β-actin at different times posttransfection. The levels of DI-EGFP RNA and 18S rRNA were similar between the groups at the same time point as quantified by RT-qPCR. (E) Relative levels of *in vivo* fusion protein synthesis based on the results of the right panel in (D). The values shown are relative to the amount of synthesis in the presence of His-β-actin at each time point. (F) Left panel: diagram showing the experimental procedures to determine the effect of N protein on the translation efficiency of BCoV nsp1 *in vivo*. Right panel: immunoblotting showing the synthesis of BCoV nsp1 in the presence of N protein or His-β-actin at different times posttransfection. The levels of viral genome (BCoV gRNA) and 18S rRNA were similar between the groups at the same time point as quantified by RT-qPCR. (G) Relative levels of BCoV nsp1 *in vivo* based on the results of the right panel in (F). The values shown are relative to the amount of synthesis in the presence of His-β-actin at each time point. Values in (B), (C), (E) and (G) represent the mean±SD (n=3) of three independent experiments. *p<0.05, **p<0.01, ***p<0.001 by an unpaired Student t test. RRL, rabbit reticulocyte lysate; Ipt. DI., input DI-EGFP RNA transcript; pt, posttransfection; N, N protein; β, His-β-actin.

Fig. 5. Translation inhibition of cellular mRNA by N protein. (A) Left panel: *in vitro*-synthesized β-actin (top) from 1 μg of input β-actin RNA transcript with the 65-nt poly(A) tail (Ipt. β-act.) (middle), which was preincubated first with 0, 2 and 4 μM of N protein (bottom) and then subjected to *in vitro* translation in RRL. Right panel: relative levels of *in vitro*-synthesized β-actin. The values shown are relative to

965 the amount of synthesis in the absence of N protein (i.e., 0 μM of N protein). (B) Left
966 panel: *in vitro*-synthesized β-actin (top) from 1 μg of the input poly(A) tail-deficient
967 β-actin RNA transcript (Ipt. β-act.) (middle), which was preincubated with 0, 2 and 4
968 μM of N protein (bottom) and then subjected to *in vitro* translation in RRL. Right
969 panel: relative levels of *in vitro*-synthesized β-actin. The values shown are relative to
970 the amount of synthesis in the absence of N protein (i.e., 0 μM of N protein). (C)
971 Effect of expressed N protein on translation of host mRNAs *in vivo*. After mock
972 transfection or independent transfection of His-β-actin and N protein RNA transcripts
973 into HEK-293T cells in the absence or presence of actinomycin D followed by
974 [^{35}S]-methionine, equal amounts of cell lysate were analyzed by SDS-PAGE, which
975 was exposed to x-ray film (left panel) or stained with Coomassie blue (right panel).
976 The levels of host mRNA (represented by GAPDH mRNA) and 18S rRNA shown in
977 the left panel were quantified by RT-qPCR. (D) Relative levels of host protein
978 synthesis based on the results of the left panel of (C). The values shown are relative to
979 the amount of synthesis in the absence of transfection (i.e., mock transfection). Values
980 in (A), (B) and (D) represent the mean±SD (n=3) of three independent experiments.
981 ***$p<0.001$ by an unpaired Student t test. RRL, rabbit reticulocyte lysate; Ipt. β-act.,
982 input β-actin RNA transcript.
983
984 **Fig. 6. Interactions between poly(A) tail, N protein and PABP.** (A) Interactions of
985 the poly(A) tail with N protein and/or PABP in mock-infected or infected cell lysates.
986 Proteins from mock-infected or infected cell lysates interacting with a biotinylated
987 poly(A) tail were pulled down by streptavidin followed by immunoblotting using
988 antibodies against PABP and N protein. The upper and lower asterisks in lanes 1, 9
989 (from streptavidin pull-down samples of infected cell lysates) and 3 (from infected
990 cell lysates) indicate cellular PABP and coronaviral N protein, respectively; the

asterisk in lane 4 (from mock-infected cell lysates) indicates cellular PABP; the asterisks in lanes 5 and 6 indicate *E. coli*-expressed N protein and PABP, respectively; the asterisk in lane 7 indicates untagged N protein; the asterisk in lane 10 (from streptavidin pull-down samples of mock-infected cell lysates) indicates cellular PABP. (B) His-tagged PABP (left panel) and untagged N protein (right panel) were expressed in *E. coli*, analyzed by SDS-PAGE and stained with Coomassie blue. (C) Pull-down assay to determine direct binding between PABP and N protein. His-tagged PABP was bound to Ni-NTA beads and mixed with untagged N protein. The pull-down materials were detected by immunoblotting using an antibody against N protein (left panel) or PABP (right panel). (D) Pull-down assay using His-tagged N protein (left panel) or His-tagged PABP (right panel) to assess its interaction with PABP or N protein, respectively, in infected cell lysates. Bound proteins from lysates were analyzed by immunoblotting with an antibody against PABP (left panel) or N protein (right panel). The arrow indicates the position of PABP (left panel) and N protein (right panel). PD, pull down; IB, immunoblotting.

Fig. 7. Interactions of poly(A) tail and N protein with cellular eIF4G and coronavirus nsp9. (A) The poly(A) tail interacts with cellular eIF4G and coronavirus nsp9. Infected cell lysates were incubated with the biotinylated poly(A) tail and pulled down by streptavidin followed by immunoblotting with antibodies against eIF4G (left panel) and nsp9 (right panel). Coronavirus nsp9 (12 kDa) and cellular eIF4G (220 kDa), indicated by an arrow in lane 1 of the left and right panels, respectively, were identified. (B) Ni-NTA beads pull-down assay using the His-tagged N protein followed by immunoblotting with an antibody against eIF4G to determine interaction between N protein and eIF4G. The arrow indicates the position of 220-kDa eIF4G. (C) Protein G beads pull-down assay followed by immunoblotting with an antibody

against eIF4G to determine interaction between N protein and eIF4G. The arrow indicates the position of 220-kDa eIF4G. (D) Ni-NTA beads pull-down assay using the His-tagged N protein followed by immunoblotting with an antibody against nsp9 to determine interaction between N protein and nsp9. The arrow indicates the position of 12-kDa nsp9. PD, pull down; IB, immunoblotting.

Fig. 8. Interactions of the poly(A) tail and N protein with cellular eIF4E. (A) Interaction of the poly(A) tail-bound N protein with eIF4G and eIF4E in mock-infected cells. Lanes 1-6 in panels 1 and 2: A fixed concentration (25 nM) of biotinylated RNA consisting of 19 non-poly(A) nts followed by the 65-nt poly(A) tail was first incubated with increasing amounts (2, 4, 6 μM) of PABP (lanes 1-3) or N protein (lanes 4-6) and then with mock-infected cell lysates followed by a streptavidin pull-down assay and immunoblotting. Values in panels 1 and 2 represent the mean percentage of three independent experiments but SD is not shown. Lanes 1-6 in panels 3 and 4: Detection of input PABP (panel 3) and N protein (panel 4) bound by biotinylated RNA. A fixed concentration (25 nM) of biotinylated RNA consisting of 19 non-poly(A) nts followed by the 65-nt poly(A) tail was incubated with increased amounts (2, 4, 6 μM) of PABP (lanes 1-3) or N protein (lanes 4-6) followed by a streptavidin pull-down assay and immunoblotting. Lanes 1-6 in panels 5 and 6: Detection of eIF4G and eIF4E by immunoblotting from uninfected cell lysates used for the aforementioned streptavidin pull-down assay. Lane 7 in panels 1 and 2: The N protein was incubated with mock-infected cell lysates followed by an Ni-NTA bead pull-down assay and immunoblotting. Lane 8 in panels 1 and 2: Biotinylated RNA consisting of 19 non-poly(A) nts followed by the 65-nt poly(A) tail was incubated with mock-infected cell lysates followed by a streptavidin pull-down assay and immunoblotting. Lanes 7-8 in panels 5 and 6: Detection of eIF4G and eIF4E from

1043 mock-infected cell lysates used for the aforementioned Ni-NTA bead (lane 7) or
1044 streptavidin (lane 8) pull-down assay by immunoblotting. (B) Interaction of the
1045 poly(A) tail with eIF4G and eIF4E in BCoV-infected cells. Panels 1-4: Lanes 3-6,
1046 biotinylated RNA consisting of 19 non-poly(A) nts followed by the 65-nt poly(A) tail
1047 was incubated with BCoV-infected cell lysates collected at 0, 8, 16 and 24 hpi
1048 followed by a streptavidin pull-down assay and immunoblotting. Lane 1, uninfected
1049 cell lysates only; Lane 2, infected cell lysates only. Lanes 7 and 8, the streptavidin
1050 beads were incubated with infected (lane 7) or uninfected (lane 8) cell lysates
1051 followed by a streptavidin pull-down assay and immunoblotting. Values in panels 1
1052 and 2 represent the mean percentage of three independent experiments but SD is not
1053 shown. Panels 5 and 8: Detection of N protein, nsp9, eIF4G and eIF4E by
1054 immunoblotting from uninfected or infected cell lysates used for the aforementioned
1055 streptavidin pull-down assay. PD, pull down; IB, immunoblotting. hpi, hour
1056 postinfection.
1057
1058 **Fig. 9. Proposed model for the regulation of gene expression in coronaviruses.** (A)
1059 The poly(A) tail of the coronavirus genomic RNA binds to PABP followed by eIF4G
1060 and eIF4E, leading to translation. (B) N protein can bind to the poly(A) tail of
1061 coronavirus genomic RNA and interact with eIF4G but not with eIF4E, leading to
1062 translation inhibition.
1063

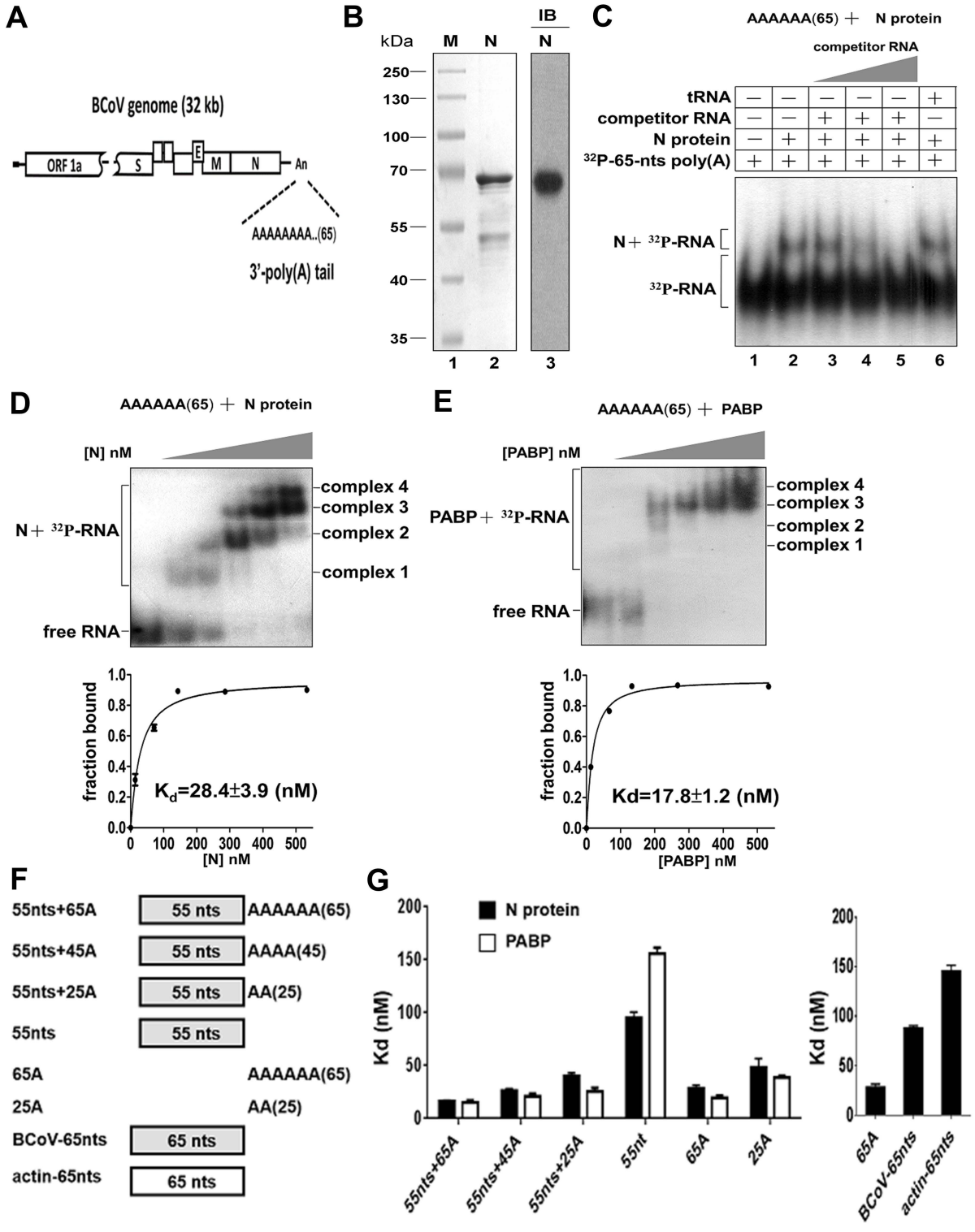

Fig. 1

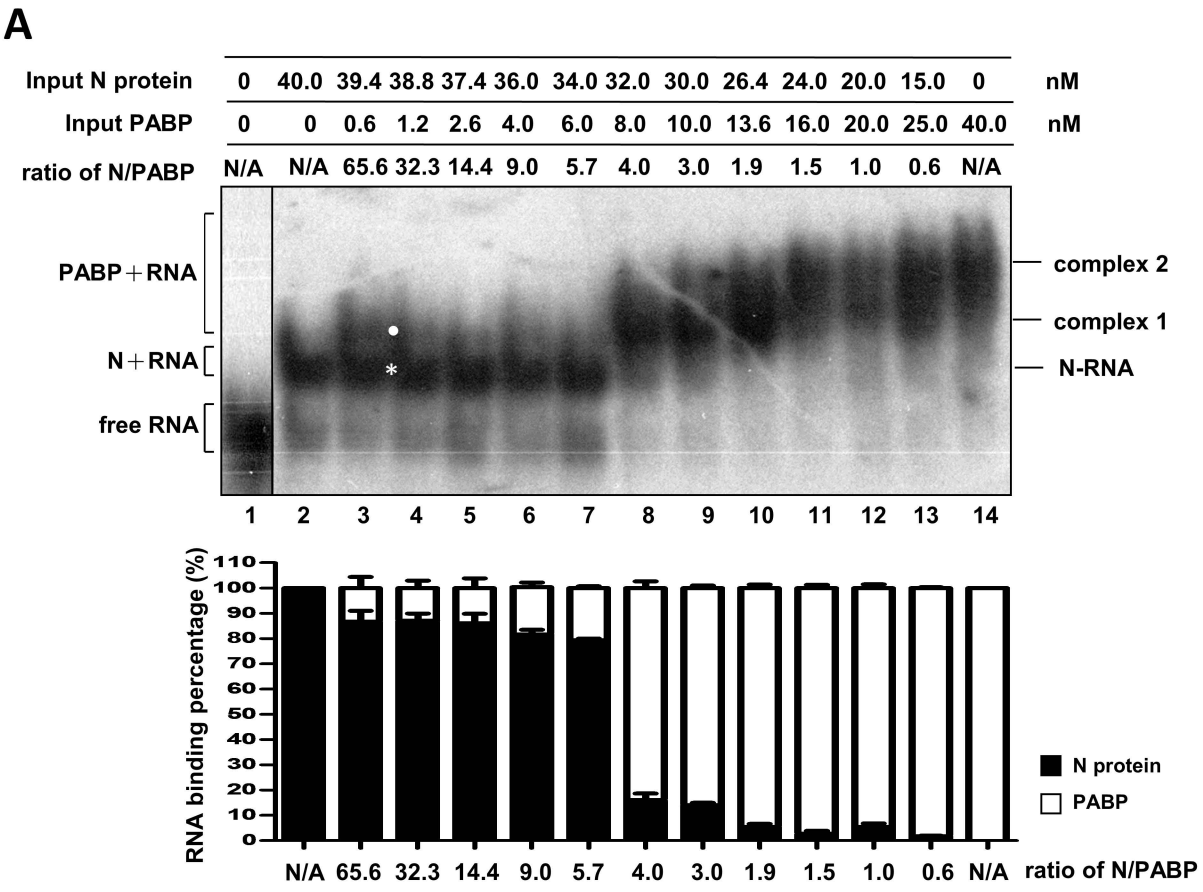

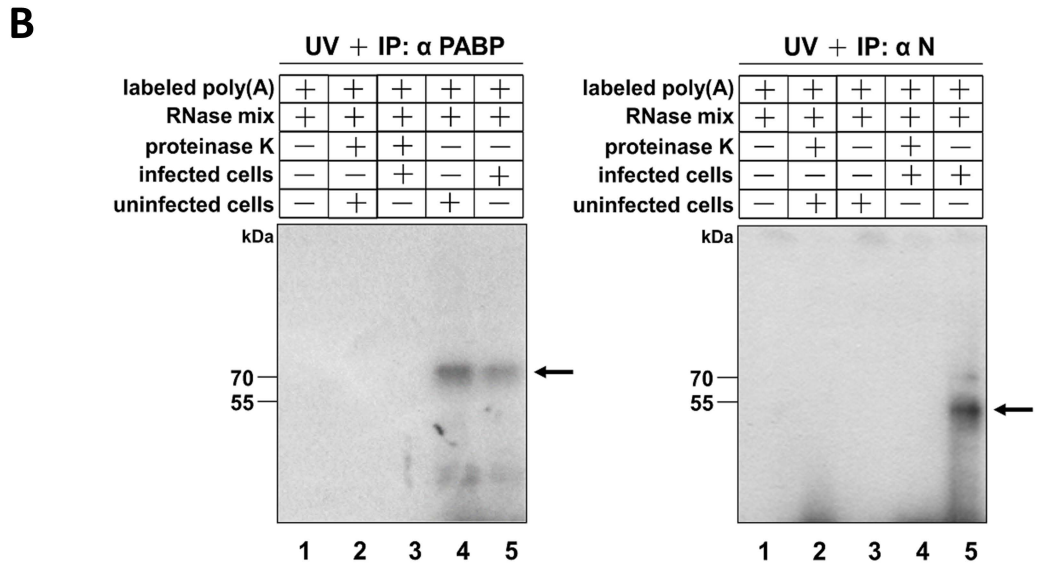

Fig. 2

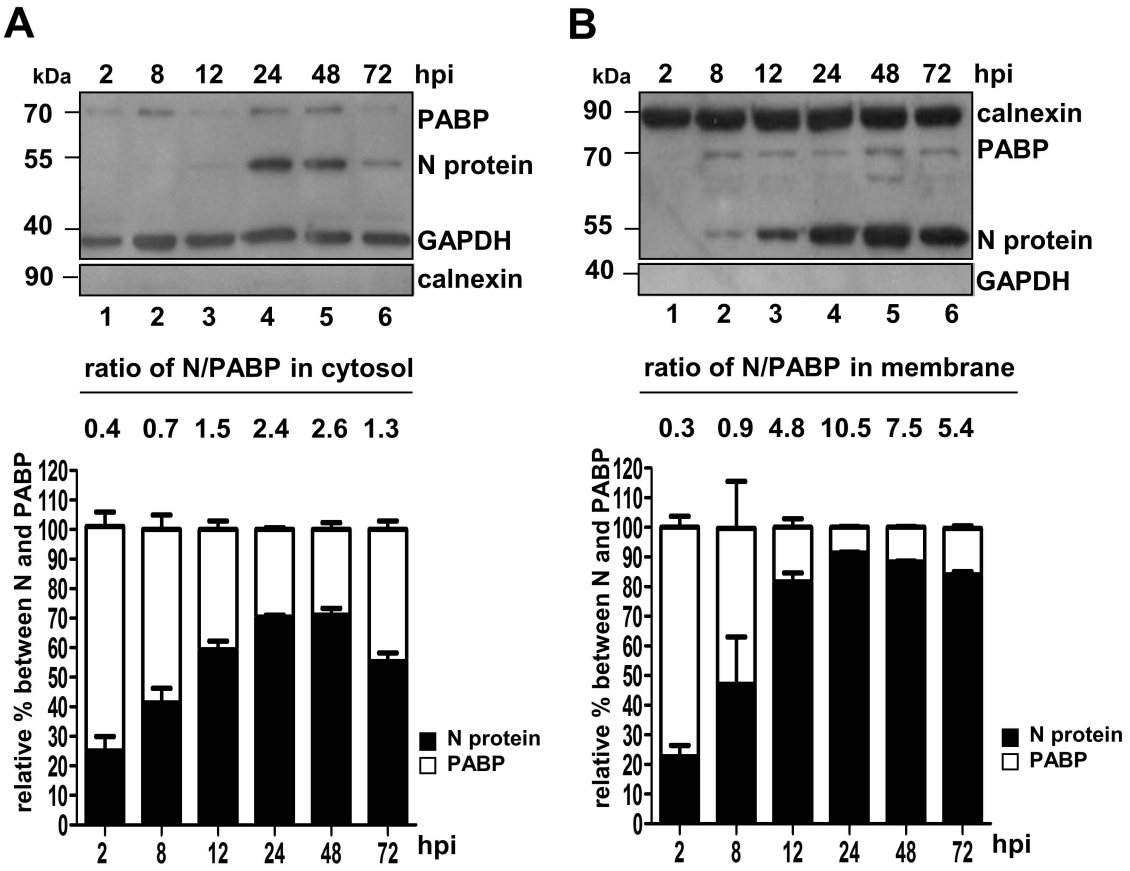

Fig. 3

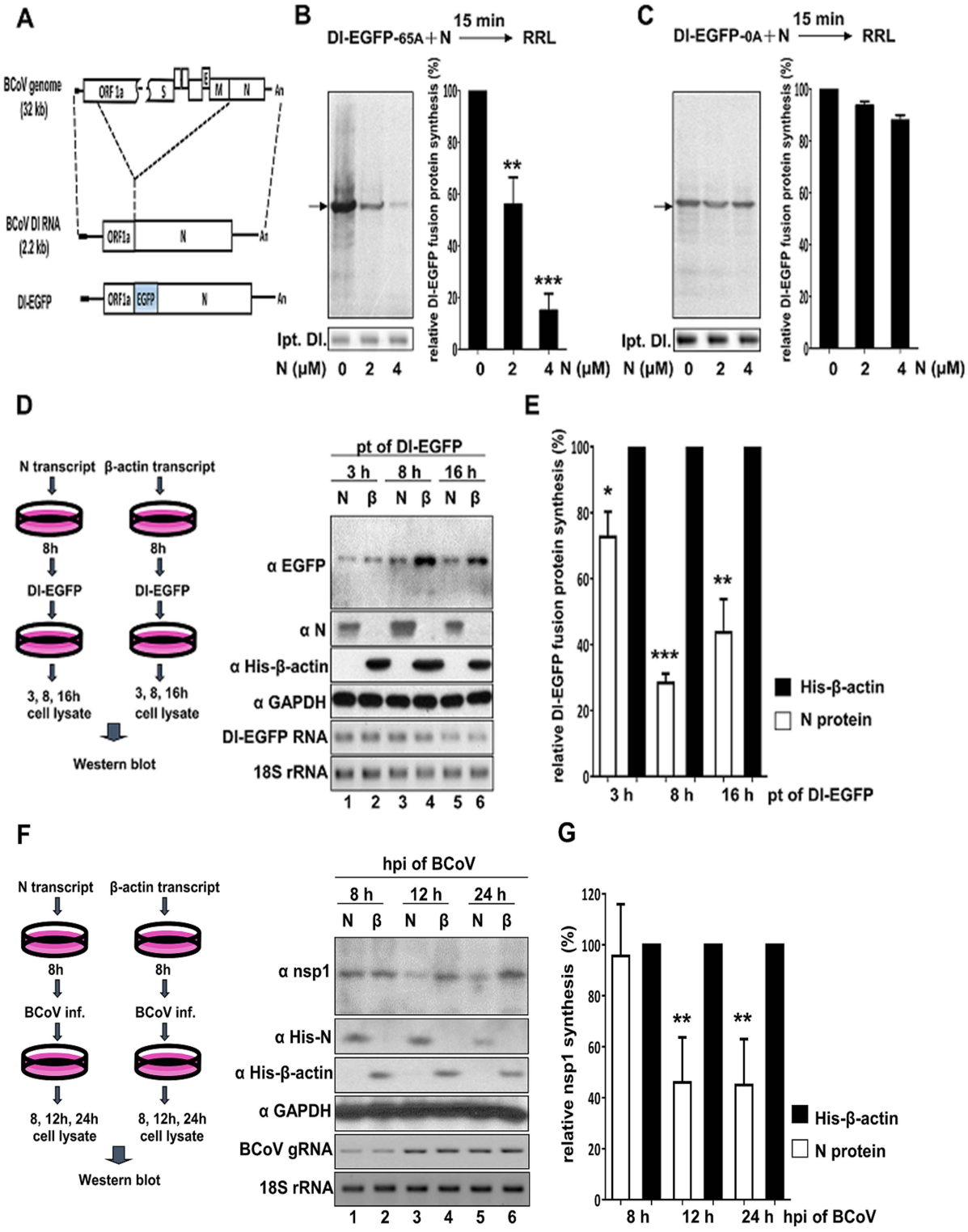

Fig. 4

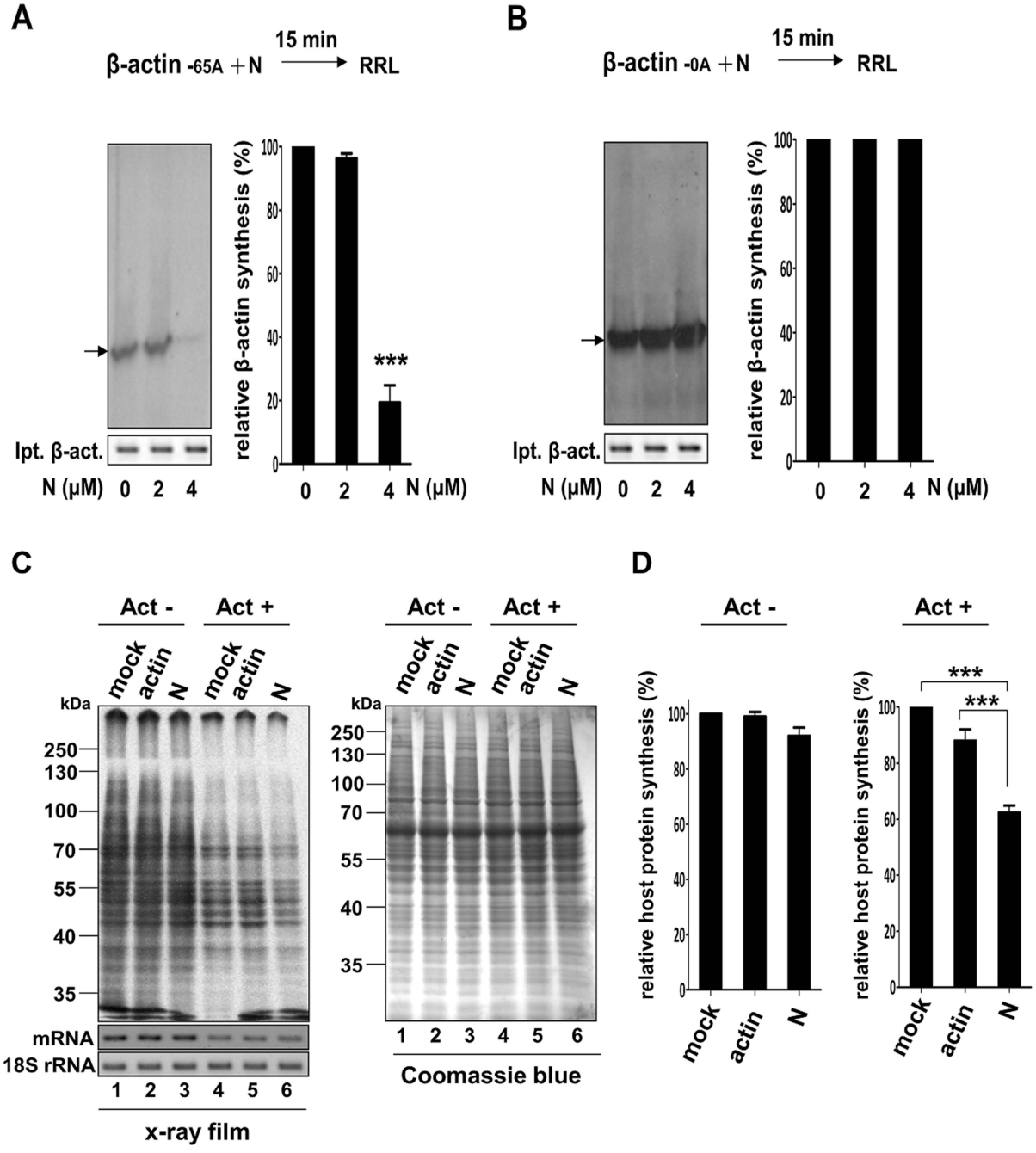

Fig. 5

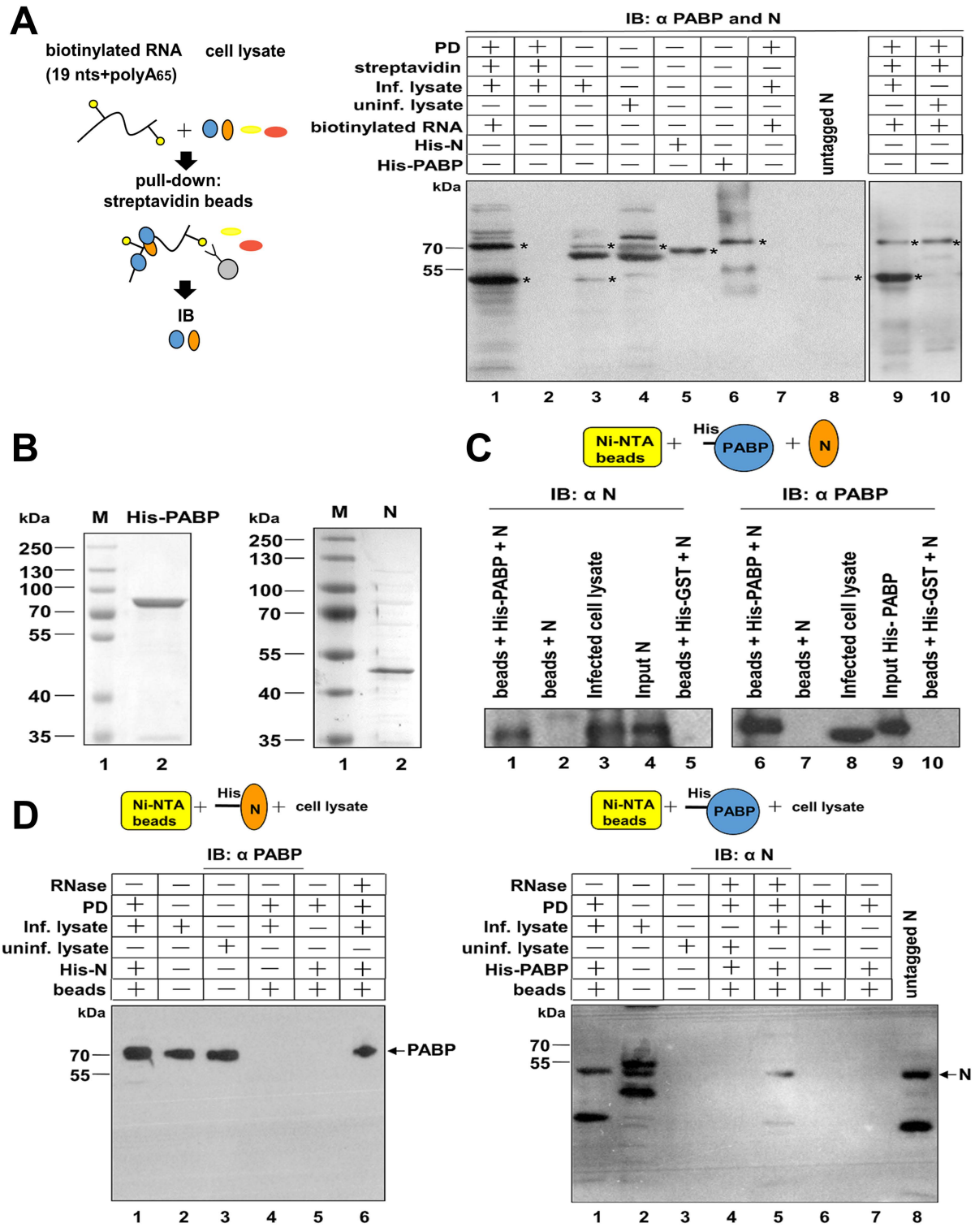

Fig. 6

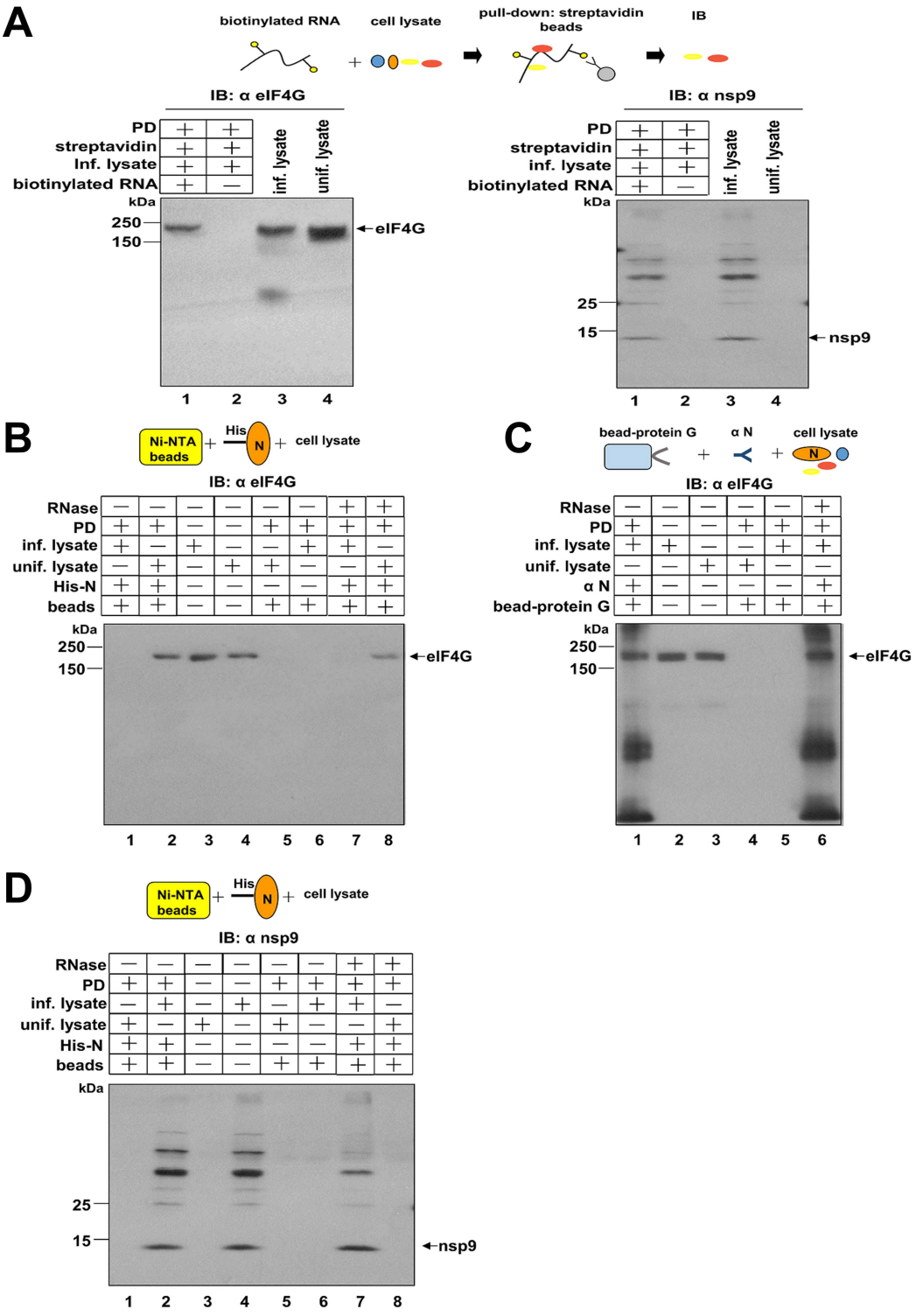

Fig. 7

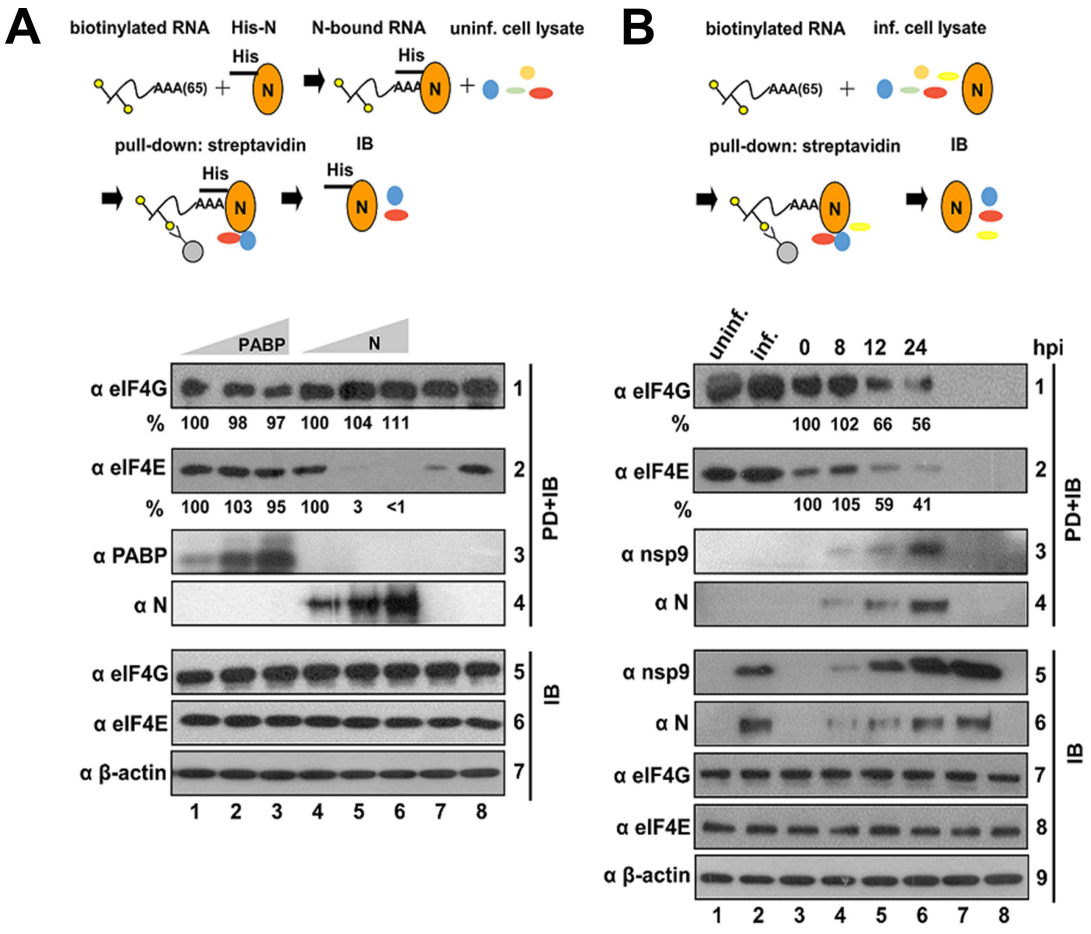

Fig. 8

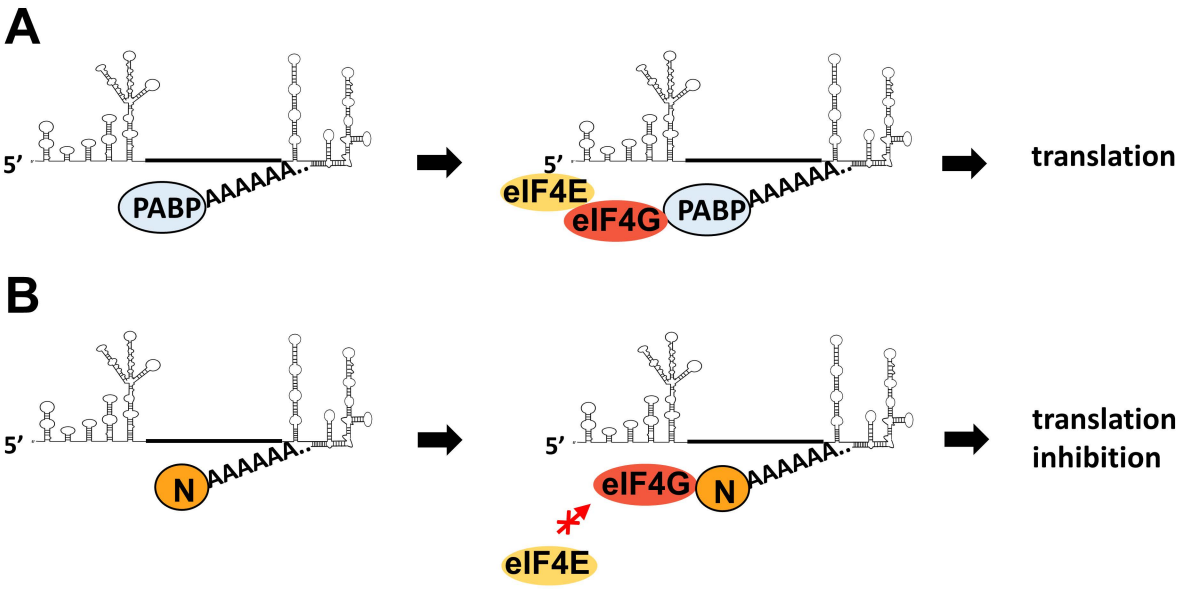

Fig. 9